Spontaneous aminolytic cyclization and self-assembly of dipeptide methyl esters in water

Charalampos G. Pappas [a, b‡*] *Nadeesha Wijerathne* [b, c, d,‡] *Jugal Kishore Sahoo,*[a‡] *Ankit Jain,*[b] *Daniela Kroiss,*[b,e] *Ivan R. Sasselli,*[a] *Ana Sofia Pina,*[b] *Ayala Lampel* [b] *and Rein V. Ulijn* [b, c, d, e*]

[a] Dr. Charalampos G. Pappas, Dr. Jugal Kishore Sahoo, Dr. Ivan R. Sasselli, Department of Pure and Applied Chemistry, Technology and Innovative Centre, University of Strathclyde, Glasgow, G1 1RD, UK.

Email: c.pappas@rug.nl

[b] Dr. Nadeesha Wijerathne, Dr. Ankit Jain, Dr. Daniela Kroiss, Dr. Ana Sofia Pina, Dr. Ayala Lampel, Prof. Rein V. Ulijn, Advanced Science Research Center (ASRC) at the City University of New York (CUNY), 85 St Nicholas Terrace, New York, 10031, USA.

Email: rein.ulijn@asrc.cuny.edu

[c] Dr. Nadeesha Wijerathne, Prof. Rein V. Ulijn, Hunter College, Department of Chemistry, CUNY, 695 Park Avenue, New York, 10065, USA.

[d] Dr. Nadeesha Wijerathne, Prof. Rein V. Ulijn, Ph.D. Program in Chemistry, The Graduate Center of the City University of New York, New York, NY, 10016, USA.

[e] Dr. Daniela Kroiss, Prof. Rein V. Ulijn, Ph.D. Program in Biochemistry, The Graduate Center of the City University of New York, New York, NY, 10016.

‡ - The authors contributed equally.

Abstract: Dipeptides are known to spontaneously cyclize to diketopiperazines, and in some cases these cyclic dipeptides have been shown to self-assemble to form supramolecular nanostructures. Herein, we demonstrate the *in situ* cyclization of dipeptide methyl esters in aqueous buffer by intramolecular aminolysis, leading to the formation of diverse supramolecular nanostructures. The chemical nature of the amino acid side chains dictates the supramolecular arrangement and resulting nanoscale architectures. For c[**LF**], supramolecular gels are formed, and the concentration of starting materials influences the mechanical properties of hydrogels. Moreover, by adding metalloporphyrin to the starting dipeptide ester solution, these become incorporated through cooperative assembly**,** resulting in the formation of nanofibers able to catalyse the oxidation of organic phenol in water. The approach taken here, which combines the chemically activated assembly with the versatility of short peptides might pave the way for achieving the spontaneous formation of supramolecular order and function using simple building blocks.

Chemically triggered formation of supramolecular assemblies,[1] i.e. the chemical conversion of non-associating precursors to self-assembling architectures, has gained significant interest as a means to control structural, spatial and dynamic features of supramolecular nanomaterials. Using chemical conversions to trigger self-assembly has been extensively studied by Van Esch,[2] Boekhoven,[3] Hermans,[4] Xu,[5] and us[6] amongst others, usually with the objective to trigger and manipulate the assembly of supramolecular hydrogelators. This approach provides a level of control over both kinetics (through modulating reaction rates) and thermodynamics (modulating chemical structure of building blocks), giving access to equilibrium,[6] kinetically trapped[7] or dynamically unstable supramolecular nanostructures.[8-14] A number of supramolecular functionalities[15] have been reported by using in-situ formation of self-assembly building blocks that are difficult to achieve by using conventional self-assembly approaches, including localized nanostructure formation to selectively kill cancer cells,[16] transient electronic wires,[17] and negatively charged biological membranes which act as catalysts for hydrogel formation.[18]

Peptides and peptide derivatives are attractive building blocks for the fabrication of artificial nanostructures with tremendous biological and nanotechnology applications, arising from their combinatorial diversity and biocompatibility.[19-26] Peptide sequences as short as two or three amino acids have been utilized for nanostructure formation in a sequence dependent manner using linear[27-32] or cyclic peptides.[33-36] Cyclic dipeptides (or diketopiperazines) involve the presentation of amino acid side chain functionality at the exterior of the nanostructure, thus rendering it accessible for interactions and/or functionalization. Govindaraju's group has extensively investigated their assembly, highlighting interesting properties of these systems, including the increased stability towards proteolysis.[37-39] Both supramolecular organogels[40] and hydrogels[41] have been reported based on these structures. Gazit and Reches demonstrated the spontaneous formation and self-assembly of surface-bound arrays of cyclic diphenylalanine peptide nanotubes using chemical vapor deposition.[42] Tunable nanostructures with photoluminescence properties have also been reported for cyclic dipeptides after dimerization into quantum dots.[43] More generally, cyclic dipeptides are well-known byproducts resulting from chemical degradation, through aminolysis of dipeptide esters (including aspartame), suggesting that they form spontaneously under much milder, aqueous conditions.[44, 45] Finally, short peptides and diketopiperazines have been considered as an important class of building blocks in the origin of life research and autonomous peptide oligomerization.[46]

We decided to investigate whether this known autonomous reaction can be optimized and coupled with the use of dipeptide sequences that give rise to spontaneous nanostructure formation in water, without the need of complex chemical synthesis[41] or other physicochemical routes not always compatible with self-assembly.[42] This approach combines the advantages of *in situ*, chemically activated assembly (**Scheme 1a**) and the versatility of supramolecular nanostructures based on cyclic dipeptides to produce functional minimalistic supramolecular systems (**Scheme 1b**).

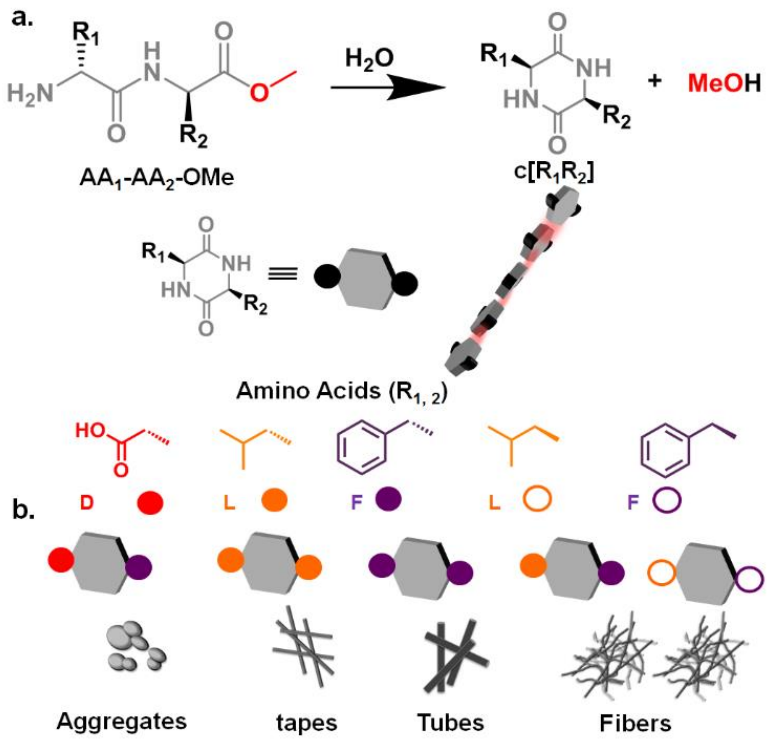

Scheme 1. (a) Spontaneous aminolysis of dipeptide methyl esters to form cyclic self-assembling moieties through intermolecular cyclisation in aqueous phosphate buffer (100 mM sodium phosphate buffer pH 8) at room temperature. Chemical structures of the dipeptide methyl ester and cyclic building blocks with different amino acid side chains depicted by single letter code, with their self-assembly propensity to form supramolecular stacks through hydrogen-bonding. (b) Schematic representation of the supramolecular organization of different cyclic dipeptides showing sequence-specific morphologies. D-amino acids (for c[**LF**]) are represented with open circles.

We started with an amphiphilic sequence, the well-known dipeptide ester, aspartame-**DF-OMe**. While we observed no noticeable macroscopic differences over time when incubating aspartame in aqueous phosphate buffer, analysis by HPLC and mass spectrometry revealed the formation of the cyclic dipeptide (c[**DF**]) to near- complete conversion within 24 hours (**Figure 1b**). Building on this observation, we then investigated a variety of homo- and hetero dipeptide methyl esters, varying the amino acid side chain (**$R_{1,2}$=** - **D**, **L**, **F**). In all cases, the cyclic dipeptides formed in high yield (as confirmed by LC/MS), and in several cases macroscopic changes could be observed (**Figure 1a**) which turned out to be a consequence of the formation of supramolecular assemblies of varying morphologies (fibres, tapes and tubes), as confirmed by Atomic Force Microscopy (AFM) and Transmission Electron Microscopy (TEM). The concentration used for all the dipeptide methyl esters was 20 mmol kg^{-1}, with all the reactions performed in 100 mM sodium phosphate buffer pH 8 at room temperature. Samples were vortexed for 60 s and sonicated for 120 s in order to obtain a homogenous solution and left standing at room temperature. Time dependent HPLC chromatographs and mass spectra of the final products are available in Supporting Information (**Figure S1, S2**).

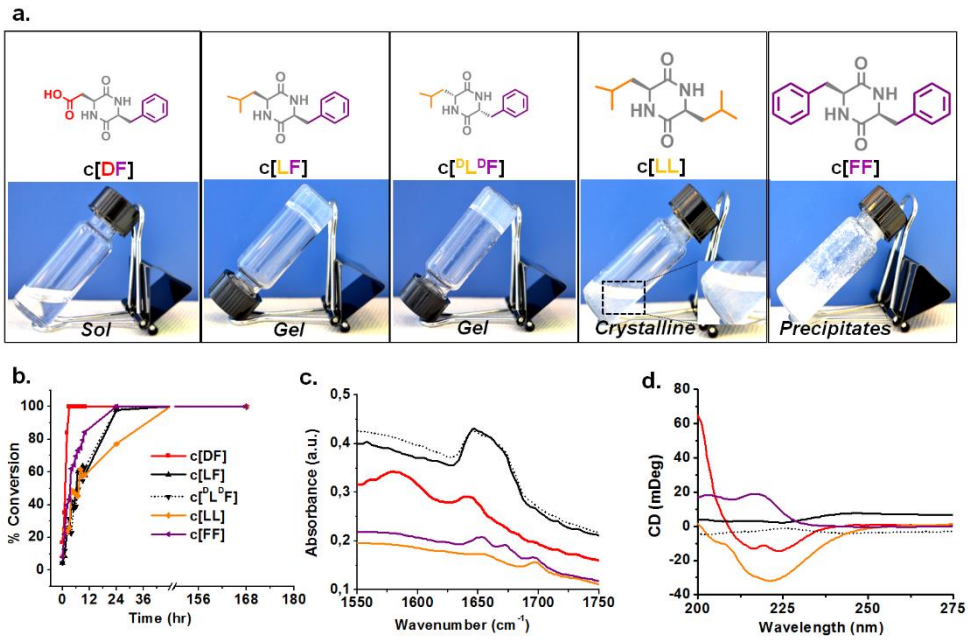

Figure 1. (a) Top panel: Chemical structure of different cyclic dipeptides; Bottom panel: Digital micrographs of various cyclic dipeptides showing sequence specific macroscopic behavior (images captured 72h after reaction). (b) Time-dependent conversion (%) determined by HPLC (monitored at 225 nm) of the formation of cyclic dipeptides catalyzed from corresponding dipeptide methyl esters in 100 mM sodium phosphate buffer pH 8 at room temperature. (c) FT-IR and (d) CD spectra of cyclic dipeptides after 72h of reaction. FT-IR was performed in D_2O phosphate buffer.

In order to investigate whether the preformed cyclic structures can accelerate the aminolysis, seeding experiments were performed by adding 5 mol % of the cyclic dipeptides at the early of the process. Time-dependent HPLC revealed no significant effects on the rate of the formation (**Figure S3**). For hydrophobic dipeptides, dramatic changes were macroscopically observed. In case of **LF-OMe**, a translucent gel-like material was formed after 24 hours, while for c[**LL**] and c[**FF**] precipitates were observed (**Figure 1a**). As expected, for the dipeptide methyl ester containing D-amino acids (**^{D}L^{D}F-OMe**), a translucent hydrogel was obtained, which could not be distinguished from that produced from the all L-peptide (**Figure 1a**). It is worth mentioning that the formation of higher linear or cyclic oligomers under the conditions tested was not observed using HPLC/MS. The cyclic peptide formation was also

confirmed by ^{1}H NMR spectroscopy (**Figure S4**). We investigated changes in amide conformation and interactions of the peptide backbones, as a result of spontaneous intermolecular dipeptide cyclisation using FT-IR spectroscopy (**Figure 1c**). The FT-IR spectra of the dipeptide esters immediately after dissolving did not show significant evidence of ordered hydrogen bonding networks (**Figure S5**); the 1675 cm^{-1} peak observed in c[**FF**] and c[**LF**] may be attributed to the presence of residual trifluoroacetic acid (TFA).[27] After the reaction was completed, two characteristic peaks were observed for c[**DF**]. A first one at 1580 cm^{-1}, which can be assigned to the carboxylate group, suggested deprotonation of the side chain and a second broad peak at 1650 cm^{-1} revealing hydrogen-bonding interactions, involving the amide groups. A broader peak with higher intensity was identified for c[**LF**] and c[^{D}**L**^{D}**F**] respectively, suggesting that aggregation takes place *via* intermolecular hydrogen bonding of the amide groups, giving rise to the formation of supramolecular fibers and hydrogels.[27] For c[**FF**] and c[**LL**], hydrogen bonding interactions also played a role in the self-assembly.

In order to gain insights into the supramolecular chirality of the cyclic dipeptides and the role of the chiral ordering of the amino acid residues on the spontaneous assembly, Circular Dichroism (CD) spectroscopy was also used (**Figure 1d**). The CD spectrum of c[**DF**] showed a weak negative peak around 220 nm. A dramatic change was observed for c[**LL**], exhibited an intense negative CD signal, as this was evidenced by the appearance of a peak at 222 nm (**Figure 1d**), highlighting the supramolecular chiral ordering of leucine amino acid residues within the assembly. Reduced CD signals were observed for the c[**LF**] and c[^{D}**L**^{D}**F**] hydrogels, with opposite chirality. The cyclic diphenylalanine (c[**FF**]) showed a positive peak around 220 nm, which can be attributed to the chiral environment of the phenylalanine amino acid residues. The CD spectra of the dipeptide esters immediately after dissolving showed limited chiral supramolecular arrangement (**Figure S6**). LD spectra of the cyclic dipeptides showed minimal contribution (**Figure S7**). HT values are also available in Supporting Info (**Figure S8).**

Time-dependent AFM imaging was used to investigate the structural transitions at the microscopic level before and after the formation of the cyclic dipeptides (**Figure 2a**). Analysis by AFM showed the formation of amorphous aggregates in the case of c[**DF**], with no distinct supramolecular transition observed after 72 hours. For c[**LF**] and c[^{D}**L**^{D}**F**]), the dipeptide esters showed ill-defined aggregates. Over time, fibrillar structures were formed, which increased both in length and density during the formation of hydrogels. For the cyclic homodipeptides, dileucine (c[**LL**]) or diphenylalnine (c[**FF**]), at the early of the process, amorphous aggregates were detected. A supramolecular reconfiguration to form tape and tubular assemblies was noticed respectively, which is in agreement for the latter with previous observations using CVD.[42] TEM images (**Figure 2b)** of the final assemblies further support the supramolecular structures found using AFM. The spectroscopic and microscopic observations highlight that the methyl ester precursors do not adopt well-defined supramolecular arrangements, however they contain sufficient chemical information to trigger the formation of diverse supramolecular structures (fibers, tapes and tubes) upon cyclization, as observed for (non)-symmetrically hydrophobic dipeptides (c[**LL**], c[**LF**], c[^{D}**L**^{D}**F**], c[**FF**]). For the negatively charged sequence (c[**DF**]) aggregates were observed.

Having demonstrated the formation of supramolecular nanostructures by *in situ* cyclisation and assembly, we subsequently investigate the possibility to trigger the formation of hydrogels of c[**LF**] with tunable mechanical properties. We hypothesized that this should be feasible by simply varying the starting material concentrations. In

order to demonstrate this, we monitored the stiffness of c[**LF**] hydrogels at four different concentrations (5, 10, 20 and 40 mmol kg^{-1}) using rheology. The 40 mmol kg^{-1} hydrogel exhibited almost three-fold increase in stiffness (G' (storage modulus) ≈ 7000 Pa) compared to the 20 mmol kg^{-1} (G' ≈ 2000 Pa). The 10 mmol kg^{-1} hydrogel showed a G' of 1000 Pa, while the sample at the lowest concentration (which also represents the minimum gelation concentration) was not sufficiently stable for accurate analysis (**Figure 3a, Figure S9, S10**). The 20 mmol kg^{-1} hydrogel was used to further investigate its thermal stability (temperature range from 25°C to 70°C) and self-healing propensity under a constant strain (0.3%). It was observed that the hydrogel retained its stability even at 70°C maintaining the stiffness (G') unchanged (**Figure 3b**). The self-healing ability was then performed by measuring G' and G" at a constant stress for 120 s, six cycles at 120 s intervals for recovery. The gel state and G' were kept intact after completion of six cycles but the recovery time was increased in each cycle (**Figure 3c**).

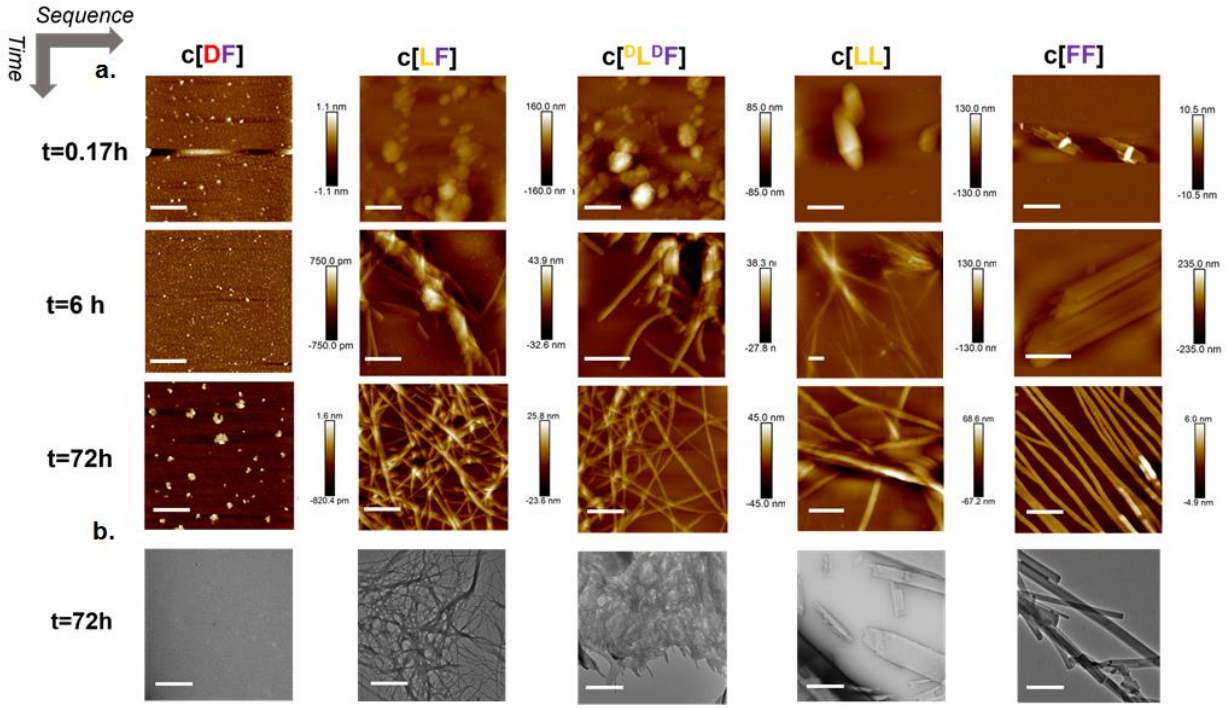

Figure 2. (a) Time-dependent AFM images of the cyclization reaction after 10 minutes, 6 and 72 hours for c[**DF**], c[**LF**], c[^{D}**L**^{D}**F**], c[**LL**] and c[**FF**]. (b) TEM images after 72 hours, Scale Bar: 500 nm.

Multi-component co-assembly has been used to generate new materials with enhanced complexity and functionalities.[47-50] Consequently, we investigated whether spontaneous cyclisation-driven co-assembly may be used to introduce functional components into these structures. Thus, dipeptide methyl esters were used to investigate co-assembly with a cationic metalloporphyrin derivative, tetramethylpyridylporphyrin iron complex (Fe^{III}-TMPyP) (**Figure S11**), which has been previously reported to exhibit peroxidase-like activity when bound to an antibody.[51] Out of five cyclic peptides in the study, c[**LF**] showed promising co-assembly behavior with Fe^{III}-TMPyP (**Figure 4a**),[52] without significantly disturbing the hydrogen-bonding pattern as evidenced using FT-IR spectroscopy (**Figure S12**). The other cyclic dipeptides could not retain their supramolecular nanostructure upon incorporation of porphyrin (**Figure S13**). Structural characterization using AFM (**Figure 4c**) revealed that

incorporation of Fe^{III}-TMPyP into c[**LF**] and c[^{D}**L**^{D}**F**], exhibited a fibrillar network with an apparently more aligned pattern (**Figure S14**) compared to the fibers without porphyrin. CD experiments (**Figure S15**) revealed an increase in the chiral environment of c[**LF**]-Fe^{III}-TMPyP in 200-250 nm range. This increase might be attributed to the helical induction of porphyrin in in the presence of c[**LF**].

We then study the catalytic efficiency of peptide-metalloporphyrin complexes on the oxidation of pyrogallol (**Figure 4b**). The c[**LF**]-porphyrin nanofibers showed enhanced catalytic activity compared to Fe^{III}-TMPyP monomers, suggesting that the fibrous hydrogel network aids in accelerating the oxidation reaction than the Fe^{III}-TMPyP molecules present in solution. We employed three different concentrations of c[**LF**] (1, 2 and 5 mmol kg^{-1}) in the presence of 1 μM solution of Fe^{III}-TMPyP. The peroxidase activity of resulting samples was tested for oxidation of pyrogallol by monitoring the oxidation product by time course UV-Visible absorbance at 420 nm (**Figure S16**). The control measurements were carried out with a sample containing only Fe^{III}–TMPyP and another one with only substrate (1 mM pyrogallol) to ensure that the spontaneous oxidation of pyrogallol is not contributing to catalytic effects. The hydrogel formed at 5 mmol kg^{-1} c[**LF**] (**Figure S17**), showed the highest initial rate of oxidation. The variation of the initial rates may be attributed to the morphological changes as demonstrated using AFM (**Figure 4c**), where increasing peptide concentration leads to the formation of more ordered assemblies, thus the well-aligned arrangement of Fe^{III}-TMPyP *via* nanofiber network enhanced its catalytic activity by providing access to more active sites for catalysis. The rate of oxidation of pyrogallol was the lowest compared to the rates of porphyrin containing samples (Figure S16). Furthermore, the Lineweaver-Burk plot was constructed for the 5 mmol kg^{-1} c[**LF**] hydrogel and 1 μM Fe^{III}-TMPyP in order to calculate the steady-state kinetic parameters (Figure 4b). The Michaelis constant Km and the catalytic constant kcat values were found to be 3.4 mM and 158 min^{-1} respectively. The efficiency of the process kcat/Km (4.7 x 104 M^{-1} min^{-1}) is comparable to previous reports involving much more complex antibody stabilized porphyrin structures. In our system, we were able to incorporate porphyrins and use supramolecular peptide fibers as templates for chromophore localization through a simplistic design with equivalent efficiencies.

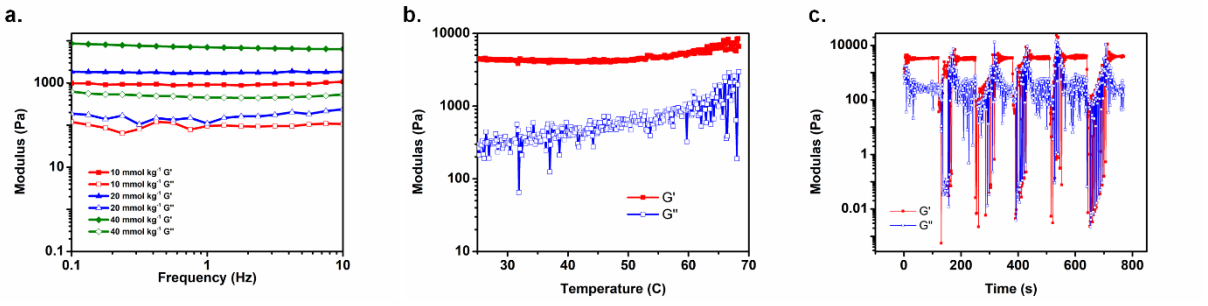

Figure 3. (a) Plot comparing the stiffness of different concentrations (10, 20 and 40 mmol kg^{-1}) of c[**LF**] gels in 100 mM sodium phosphate buffer pH 8 after 72 hours of the reaction (b) Temperature sweep measurements and (c) Self-healing measurements of 20 mmol kg^{-1} of c[**LF**].

In summary, we have demonstrated spontaneous formation of highly ordered supramolecular assemblies, as a result of *in situ* dipeptide cyclisation in aqueous media, resulting in a variety of supramolecular architectures (fibers, tubes, tapes). The nanostructures generated through co-assembly between c[**LF**] and Fe^{III}–TMPyP have shown the potential to function as catalysts in oxidation of pyrogallol. Cyclic dipeptides have been previously suggested as antimicrobial and antiviralagents[53, 54] and this study might pave the way for spontaneous fabrication of peptide nanostructures with the desired structure and function. The autonomous formation of supramolecular assemblies described here involving the formation of amide bonds, might also find interest in a prebiotic manner, as the formation of diketopiperazines is considered as a probable route for prebiotic peptide formation.[46]

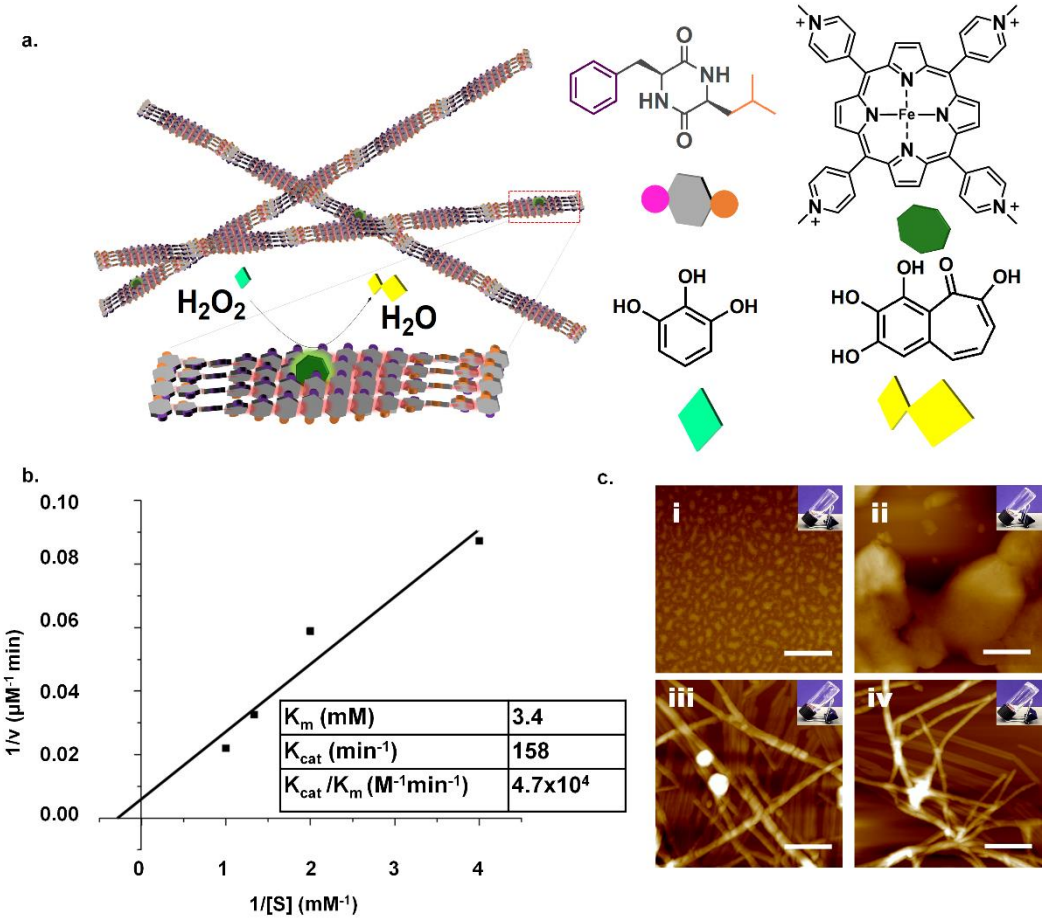

Figure 4. (a) Schematic representation of the co-assembly propensity of dipeptide hydrogel c[**LF**] and metalloporphyrin (FeIII–TMPyP) and the catalytic activity of c[**LF**]-Fe^{III}–TMPyP nanostructures on oxidation of pyrogallol. (b) Lineweaver burk plot for peroxidase-like activity of 5 mmol kg^{-1} c[**LF**]- [Fe^{III}–TMPyP] for the oxidation of pyrogallol. (c) AFM images of different concentrations of c[**LF**] i. 0 (control) ii. 1 iii. 2 and iv. 5 mmol kg^{-1} co-assembled with 1 μM Fe^{III}–TMPyP, scale bar 500 nm.

Acknowledgements

The research leading to these results has received funding from the European Research Council under the European Union's Seventh Framework Programme (FP7/2007–2013) EMERgE/ERC (Grant Agreement Number 258775) and US Air Force (AFOSR, grant FA9550-19-1-0111)).

Keywords: supramolecular chemistry • Peptide Self-assembly • spontaneous hydrogelation • catalysis • co-assembly

References

[1] F. Trausel, F. Versluis, C. Maity, J. M. Poolman, M. Lovrak, J. H. van Esch, R. Eelkema, *Acc. Chem. Res.* **2016**, *49*, 1440-1447.

[2] J. Boekhoven, W. E. Hendriksen, G. J. Koper, R. Eelkema, J. H. van Esch, *Science* **2015**, *349*, 1075-1079.

[3] M. Tena-Solsona, B. Riess, R. K. Grotsch, F. C. Lohrer, C. Wanzke, B. Kasdorf, A. R. Bausch, P. Muller-Buschbaum, O. Lieleg, J. Boekhoven, *Nat. Commun.* **2017**, *8*, 15895.

[4] A. Sorrenti, J. Leira-Iglesias, A. Sato, T. M. Hermans, *Nat. Commun.* **2017**, *8*, 15899.

[5] Z. Yang, H. Gu, D. Fu, P. Gao, J. K. Lam, B. Xu, *Adv. Mater.* **2004**, *16*, 1440-1444.

[6] C. G. Pappas, R. Shafi, I. R. Sasselli, H. Siccardi, T. Wang, V. Narang, R. Abzalimov, N. Wijerathne, R. V. Ulijn, *Nat. Nanotechnol.* **2016**, *11*, 960-967.

[7] A. R. Hirst, S. Roy, M. Arora, A. K. Das, N. Hodson, P. Murray, S. Marshall, N. Javid, J. Sefcik, J. Boekhoven, J. H. van Esch, S. Santabarbara, N. T. Hunt, R. V. Ulijn, *Nat. Chem.* **2010**, *2*, 1089-1094.

[8] B. A. Grzybowski, W. T. Huck, *Nat. Nanotechnol.* **2016**, *11*, 585-592.

[9] E. Te Brinke, J. Groen, A. Herrmann, H. A. Heus, G. Rivas, E. Spruijt, W. T. S. Huck, *Nat. Nanotechnol.* **2018**, *13*, 849-855.

[10] S. Maiti, I. Fortunati, C. Ferrante, P. Scrimin, L. J. Prins, *Nat. Chem.* **2016**, *8*, 725-731.

[11] M. Araújo, B. Escuder, ChemistrySelect **2017**, *2*, 854-862.

[12] J. H. van Esch, R. Klajn, S. Otto, *Chem. Soc. Rev.* **2017**, *46*, 5474-5475.

[13] J. Leira-Iglesias, A. Tassoni, T. Adachi, M. Stich, T. M. Hermans, *Nat. Nanotechnol.* **2018**, *13*, 1021-1027.

[14] R. K. Grotsch, C. Wanzke, M. Speckbacher, A. Angi, B. Rieger, J. Boekhoven, *J. Am. Chem. Soc.* **2019**, *141*, 9872-9878.

[15] E. Mattia, S. Otto, *Nat. Nanotechnol.* **2015**, *10*, 111-119.

[16] J. Zhou, X. Du, C. Berciu, H. He, J. Shi, D. Nicastro, B. Xu, *Chem* **2016**, *1*, 246-263.

[17] M. Kumar, N. L. Ing, V. Narang, N. K. Wijerathne, A. I. Hochbaum, R. V. Ulijn, *Nat. Chem.* **2018**, *10*, 696-703.

[18] F. Versluis, D. M. van Elsland, S. Mytnyk, D. L. Perrier, F. Trausel, J. M. Poolman, C. Maity, V. A. le Sage, S. I. van Kasteren, J. H. van Esch, R. Eelkema, *J. Am. Chem. Soc.* **2016**, *138*, 8670-8673.

[19] S. Zhang, *Nat. Biotechnol*. **2003**, *21*, 1171-1178.

[20] W. S. Childers, A. K. Mehta, R. Ni, J. V. Taylor, D. G. Lynn, *Angew. Chem. Int. Ed.* **2010**, *49*, 4104-4107.

[21] I. W. Hamley, *Angew. Chem. Int. Ed*. **2010**, *49*, 24, 4104-4107.

[22] S. Li, A. K. Mehta, A. N. Sidorov, T. M. Orlando, Z. Jiang, N. R. Anthony, D. G. Lynn, *J. Am. Chem. Soc.* **2016**, *138*, 3579-3586.

[23] C. Chen, J. Tan, M.-C. Hsieh, T. Pan, J. T. Goodwin, A. K. Mehta, M. A. Grover, D. G. Lynn, *Nat. Chem.* **2017**, *9*, 799-804.

[24] E. Gazit, *Chem. Soc. Rev.* **2007**, *36*, 1263-1269.

[25] S. Fleming, R. V. Ulijn, *Chem. Soc. Rev.* **2014**, *43*, 8150-8177.

[26] J. Raeburn, A. Zamith Cardoso, D. J. Adams, *Chem. Soc. Rev.* **2013**, *42*, 5143-5156.

[27] P. W. J. M. Frederix, G. G. Scott, Y. M. Abul-Haija, D. Kalafatovic, C. G. Pappas, N. Javid, N. T. Hunt, R. V. Ulijn, T. Tuttle, *Nat. Chem.* **2014**, *7*, 30-37.

[28] H. Erdogan, E. Babur, M. Yilmaz, E. Candas, M. Gordesel, Y. Dede, E. E. Oren, G. B. Demirel, M. K. Ozturk, M. S. Yavuz, G. Demirel, *Langmuir* **2015**, *31*, 7337-7345.

[29] Z. Fan, L. Sun, Y. Huang, Y. Wang, M. Zhang, *Nat. Nanotechnol.* **2016**, *11*, 388-4394.

[30] M. Reches, E. Gazit, *Science* **2003**, *300*, 625-627.

[31] C. H. Görbitz, *Chem. Eur. J.* **2001**, *7*, 5153-5159.

[32] N. S. de Groot, T. Parella, F. X. Aviles, J. Vendrell, S. Ventura, *Biophys. J.* **2007**, *92*, 1732-1741.

[33] S. Manchineella, T. Govindaraju, ChemPlusChem **2017**, *82*, 88-106.
[34] A. D. Borthwick, Chem. Rev. **2012**, *112*, 3641-3716.

[35] K. Nonappa; K. Ahonen, M. Lahtinen, E. Kolehmainen, Green Chem. **2011**, *13*, 1203-1209.

[36] A. Bravo, I. Gómez-Monterrey, R. González-Muñiz, M.T. García-López, J. Chem. Soc., Perkin Trans. 1, **1991**, *12*, 3117-3120
[37] T. Govindaraju, *Supramol. Chem.* **2011**, *23*, 759-767.

[38] T. Govindaraju, M. Pandeeswar, K. Jayaramulu, G. Jaipuria, H. S. Atreya, *Supramol. Chem.* **2011**, *23*, 487-492.
[39] S. Manchineella, T. Govindaraju, *RSC Adv.* **2012**, *2*, 5539-5542.

[40] H. Geng, L. Ye, A. Y. Zhang, J. Li, Z. G. Feng, *Langmuir* **2016**, *32*, 4586-4594.

[41] A. J. Kleinsmann, B. J. Nachtsheim, *Chem. Commun.* **2013**, *49*, 7818-7820.

[42] L. Adler-Abramovich, D. Aronov, P. Beker, M. Yevnin, S. Stempler, L. Buzhansky, G. Rosenman, E. Gazit, Nat. Nanotechnol. **2009**, *4*, 849-854.

[43] K. Tao, Z. Fan, L. Sun, P. Makam, Z. Tian, M. Ruegsegger, S. Shaham-Niv, D. Hansford, R. Aizen, Z. Pan, S. Galster, J. Ma, F. Yuan, M. Si, S. Qu, M. Zhang, E. Gazit, J. Li, *Nat. Commun*. **2018**, *9*, 3217.

[44] M. PRUDEL, E. DAVÍDKOVÁ, J. DAVÍDEK, M. KMÍNEK, *J. Food Sci.* **1986**, *51*, 1393-1397.

[45] J. E. Purdie, N. L. Benoiton, *J. Chem. Soc., Perkin Trans. 2* **1973**, 14, 1845-1852.

[46] M. Nagayama, O. Takaoka, K. Inomata, Y. Yamagata, *Origins of Life* **1990**, *20*, 249-257.

[47] K. E. Inostroza-Brito, E. Collin, O. Siton-Mendelson, K. H. Smith, A. Monge-Marcet, D. S. Ferreira, R. P. Rodríguez, M. Alonso, J. C. Rodríguez-Cabello, R. L. Reis, F. Sagués, L. Botto, R. Bitton, H. S. Azevedo, A. Mata, *Nat. Chem.* **2015**, *7*, 897-904.

[48] D. M. Raymond, B. L. Nilsson, *Chem. Soc. Rev.* **2018**, *47*, 3659-3720.

[49] E. R. Draper, D. J. Adams, *Chem. Soc. Rev.* **2018**, *47*, 3395-3405.

[50] P. Makam, E. Gazit, *Chem. Soc. Rev.* **2018**, *47*, 3406-3420.

[51] H. Yamaguchi, K. Tsubouchi, K. Kawaguchi, E. Horita, A. Harada, *Chem. Eur. J.* **2004**, *10*, 6179-6186.

[52] N. K. Wijerathne, M. Kumar, R. V. Ulijn, *Chem. Eur. J.* **2019**, *25*, 11847-11851.

[53] W. S. Horne, C. M. Wiethoff, C. Cui, K. M. Wilcoxen, M. Amorin, M. R. Ghadiri, G. R. Nemerow, *Bioorg. Med. Chem.* **2005**, *13*, 5145-5153.

[54] V. Dartois, J. Sanchez-Quesada, E. Cabezas, E. Chi, C. Dubbelde, C. Dunn, J. Granja, C. Gritzen, D. Weinberger, M. R. Ghadiri, T. R. Parr, *Antimicrob. Agents Chemother.* **2005**, *49*, 3302-3310.

Supplementary Information for

Spontaneous aminolytic cyclization and self-assembly of dipeptide methyl esters in water

*Charalampos G. Pappas,[*a, b‡] Nadeesha Wijerathne [b, c, d,‡] Jugal Kishore Sahoo,[a‡] Ankit Jain,[b] Daniela Kroiss,[b,e] Ivan R. Sasselli,[a] Ana Sofia Pina,[b] Ayala Lampel[b] and Rein V. Ulijn[b, c, d, e*]*

Contents

Materials and Methods

Aspartame (DF-OMe), LL-OMe, pyrogallol, hydrogen peroxide and meso-tetrakis-(4-N-methylpyridyl) porphyrin (TMPyP) were purchased from Sigma Aldrich and used as received. All the other dipeptide methyl esters (LF-OMe, $^{D}L^{D}$F-OMe and FF-OMe) were purchased from Genscript and CS Bio. The purity was 95% and the dipeptide esters were used as TFA salts.

Sample Preparation

The concentration used for the dipeptide methyl esters (DF-OMe, LL-OMe, LF-OMe, $^{D}L^{D}$F-OMe, FF-OMe) was 20 mmol kg^{-1}. 100 mM sodium phosphate buffer at pH 8 was used to dissolve the peptide esters. The samples were vortexed for 60 s and sonicated for 120 s in order to obtain a homogenous solution. For the co-assembly experiments, 2 mM of Fe^{III}-TMPyP was mixed with 20 mmol kg^{-1} of dipeptide methyl esters in 1 ml of 100 mM sodium phosphate buffer pH 8. The samples for catalytic activity were tested in concentration of 1, 2 and 5 mmol kg^{-1} of c[**LF**] in the presence of 1 μM Fe^{III}-TMPyP. For each c[**LF**]-Fe^{III}-TMPyP hydrogel, 50 mM hydrogen peroxide was added, followed by 1 mM of pyrogallol. The product of oxidation was monitored over time using UV-Vis spectroscopy at λmax (420 nm).

Preparation of Fe^{III}-TMPyP:

Fe^{III}-TMPyP was prepared by a modified procedure reported by Yamaguchi et al. *Chem. Eur. J.* **2004**, *10*, 6179-6186. Modified procedure is as follows: 250 mg **TMPyP** (obtained commercially from Sigma Aldrich) was dissolved in 100 ml water and refluxed under nitrogen atmosphere for two hours in presence of 500 molar equivalents of $FeCl_2.4H_2O$. A visible color change from brown to green with quenching of **TMPyP** emission was observed. Solution was then cooled down to room temperature and 84 ml of 2 M sodium perchlorate solution was added to precipitate the product. The reaction mixture was then allowed to stand overnight in dark. The mixture was then centrifuged (10000 rpm, 10 mins, 5 ^{o}C) in aliquots. All aliquots were combined and washed with 50 ml of perchloric acid. This was done to remove the excess of metal ions. The paste that resulted was dried under vacuum and dissolved in acetonitrile. **Fe^{III}-TMPyP** readily dissolved in acetonitrile with undissolved excess metal salt (that persisted from the perchloric acid wash) left behind. Tetraethylammonium chloride was added in small aliquots to precipitate the compound. The precipitate formed is decanted and washed with chloroform to remove excess Tetraethylammonium chloride. The washed precipitate was then dried under vacuum to yield pure **Fe^{III}-TMPyP**. Yield =47%. HRMS: Mass calculated for **Fe^{III}-TMPyP** [$C_{44}H_{38}FeN_8^{4+}$] = 734.6211, mass obtained [$C_{44}H_{38}FeN_8^{4+}$-2H+OH]/4 (m/z=m/4) = 187.3110.

Instrumentation

High Performance Liquid Chromatography (HPLC)

A Dionex P680 HPLC system equipped with a Macherey-Nagel C18 column of 250 mm length, 4.6 mm internal diameter and 5 mm particle size was used to quantify conversions of the cyclic dipeptides. The gradient used was a linear exchange between 20% acetonitrile in water at 2.5 min to 80% acetonitrile/water. Sample preparation involved by mixing 20 μl of the dipeptides with 980 μl acetronitrile/water (50:50 mixture) containing 0.1% trifluoroacetic acid. Vortexing and sonication were also applied prior to sampling for the time-course experiments. The reactions were typically analyzed for up to 7 days with no significant compositional changes after 72 hours. Reaction monitoring stopped when changes were no longer observed using HPLC/MS.

Mass spectrometry

Samples were analyzed on an LC-MS system comprised of an Agilent 1200 LC system coupled to an Agilent 6340 ion trap mass spectrometer. Samples were injected onto an Agilent Zorbax column (SB-C8, 5 uM, 2.1 x 50 mm) using a linear gradient of 5-95% acetonitrile in water (1% formic acid) at a flow rate of 200 μL/min over 10 minutes.

Infrared Spectroscopy

For the FT-IR measurements the dipeptides were dissolved in D_2O at pD 8 and spectra were recorded after the reaction was completed (72 hours). FTIR spectra were acquired in a Bruker Vertex spectrometer with a spectral resolution of 2 cm^{-1}. The measurements were performed in a standard infrared cuvette (Harrick Scientific), in which the sample was contained between two CaF_2 windows (thickness, 2 mm) separated by a 27 mm polytetrafluoroethylene spacer.

Circular and Linear Dichroism Spectroscopy (CD, LD)

Samples were pipetted into a 0.1 mm cell and spectra were measured on a Jasco J600 spectropolarimeter with 1s integrations, a step size of 1 nm and a single acquisition with a slit width of 1 nm. The measurements were performed after the reaction was completed (72 hours).

Atomic Force Microscopy (AFM)

Samples were prepared by drop casting 20 μL of each sample onto a freshly cleaved mica substrate (G250-2 Mica sheets 1″× 1 ″× 0.006″ (Agar Scientific Ltd)) attached to an AFM support stub and left to air dry overnight in a dust-free environment, prior to imaging. The images were obtained by scanning the mica surface in air under ambient conditions using a Multimode 8 FastScan Microscope (Bruker) operated in scan assist air mode with a fastscan B tip. The AFM scans were taken at a resolution of 512 × 512 pixels. The images were analyzed using NanoScope Analysis software Version 1.40.

Rheometry

Rheological properties of c[**LF**] (5, 10, 20 and 40 mmol kg^{-1}) were assessed using an Anton Paar Physica MCR 101 rheometer with temperature controlled at 25 °C using a 10 mm vane geometry. Samples were prepared using a mold with 300 µl from each concentration. Amplitude sweeps were performed to obtain the strain for each sample to run the frequency sweeps. To ensure the measurements were made in the linear viscoelastic regime, amplitude sweeps were performed at constant frequency of 1 Hz, from shear strain 0.01–100%. Gel formation was then monitored by measuring G′ and G″ at 0.1 to 100 Hz frequency range using the sheer strain for each sample. For the temperature stability measurements, 20 mmol kg^{-1} of c[**LF**] was used under a temperature ramp from 20-70 °C with constant strain of 0.03%. For the self-healing measurements 20 mmol kg^{-1} of c[**LF**] was used for six cycles (one cycle 120 s). The G′ and G″ were measured at viscoelastic region under 0.03% strain for 60 s and 20% strain beyond the viscoelastic region to break the gel for 40 s and healing time with 20 sec.

UV-VIS spectroscopy

1 ml samples were prepared in 10mm quartz cuvette. UV-VIS absorbance spectra were recorded with a Jasco V-660 spectrophotometer at a medium scanning speed of 100 nm min^{-1}. Time dependent measurements were collected at 420 nm.

^{1}H NMR spectroscopy

^{1}H NMR spectra were acquired on a Bruker AVANCE III HD 600 MHz NMR spectrometer equipped with a 5-mm TCI cryoprobe. Samples were prepared in 1:1 ratio of H_2O: CD_3CN. All ^{1}H spectra were acquired with excitation sculpting for water suppression and the following salient acquisition parameters: 32k complex points, 1.7 sec acquisition time, 2 sec relaxation delay, 6 scans for a total of approximately 4 minutes. All spectra were processed with a 0.5 Hz exponential line broadening and baseline correction, and selected peaks were integrated manually within TopSpin 3.5. Linear peptides were used as purchased and cyclic peptides were measured after 3 days of reaction.

Transmission electron microscopy

Carbon-coated grids were purchased from Electron Microscopy Sciences. A drop (5 µl) of the sample solution was applied to the carbon-coated grid and incubated for one minute. Excess solution was removed by blotting the grid with a piece of filter paper, followed by staining with 5 µl of 2% (w/v) uranyl acetate solution for 30 seconds. After blotting excess stain solution, the grid was left to air dry. The negatively stained sample was imaged in FEI TITAN Halo TEM operating at 300 kV. Images were recorded in the low-dose mode (20 $e^{-}/Å^{2}$) on an FEI CETA 16M camera (4,096 × 4,096 pixels).

Additional Supporting Data

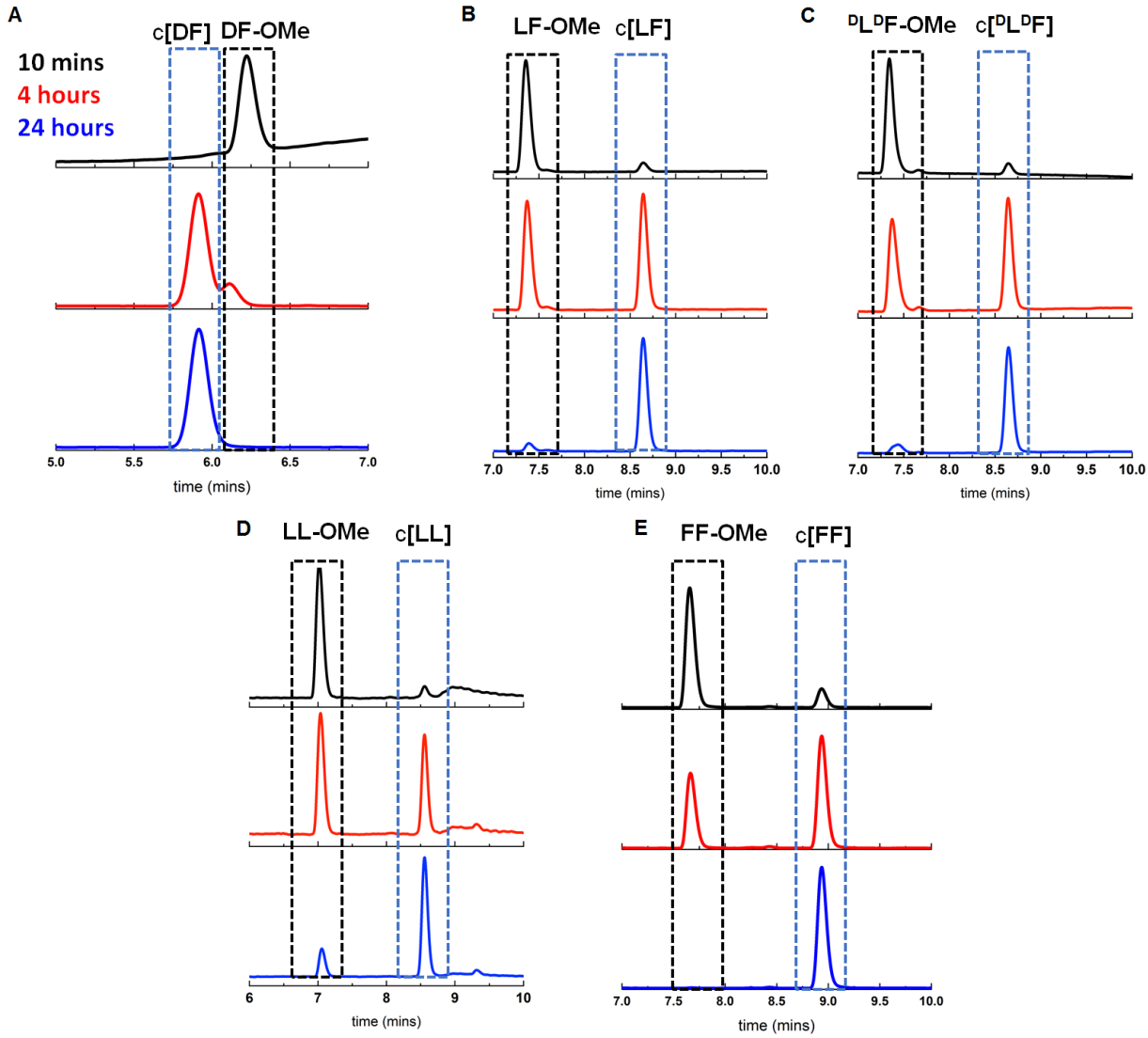

Figure S1. Time dependent HPLC chromatograms: The chromatogram (monitored at 225 nm) in black for each sequence represents the chromatogram at t=10 minutes, red after t=4 hours and blue after t= 24 hours. A) c[**DF**], B) c[**LF**], C) c[^{D}**L**^{D}**F**], D) c[**LL**], E) c[**FF**].

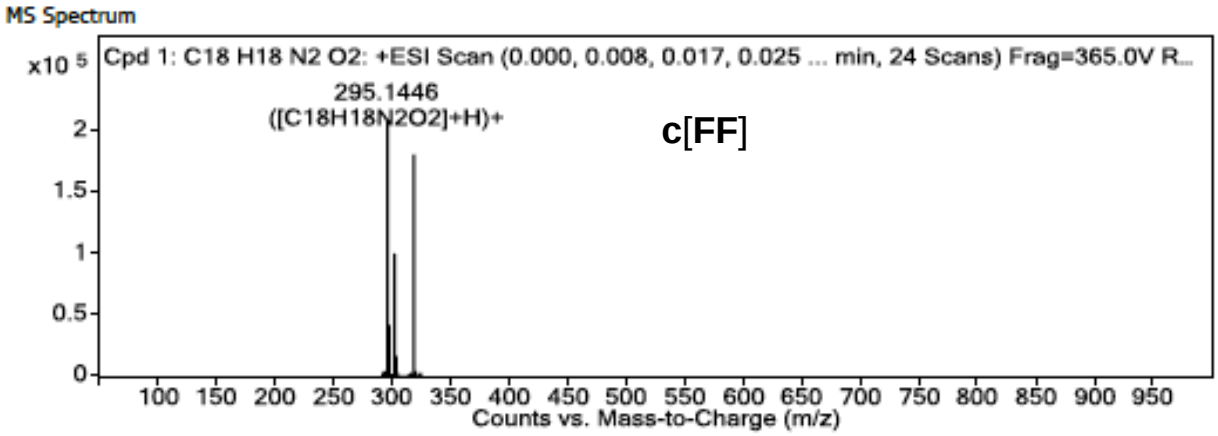
MS Spectrum
Cpd 1: C18 H18 N2 O2: +ESI Scan (0.000, 0.008, 0.017, 0.025 ... min, 24 Scans) Frag=365.0V R...
x10 5
295.1446
([C18H18N2O2]+H)+
c[FF]
Counts vs. Mass-to-Charge (m/z)

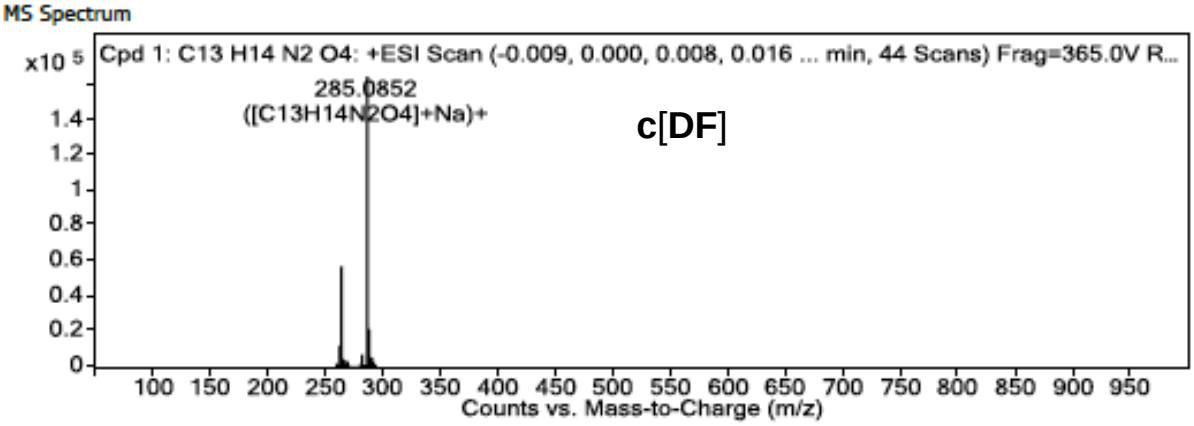
MS Spectrum
Cpd 1: C13 H14 N2 O4: +ESI Scan (-0.009, 0.000, 0.008, 0.016 ... min, 44 Scans) Frag=365.0V R...
x10 5
285.0852
([C13H14N2O4]+Na)+
c[DF]
Counts vs. Mass-to-Charge (m/z)

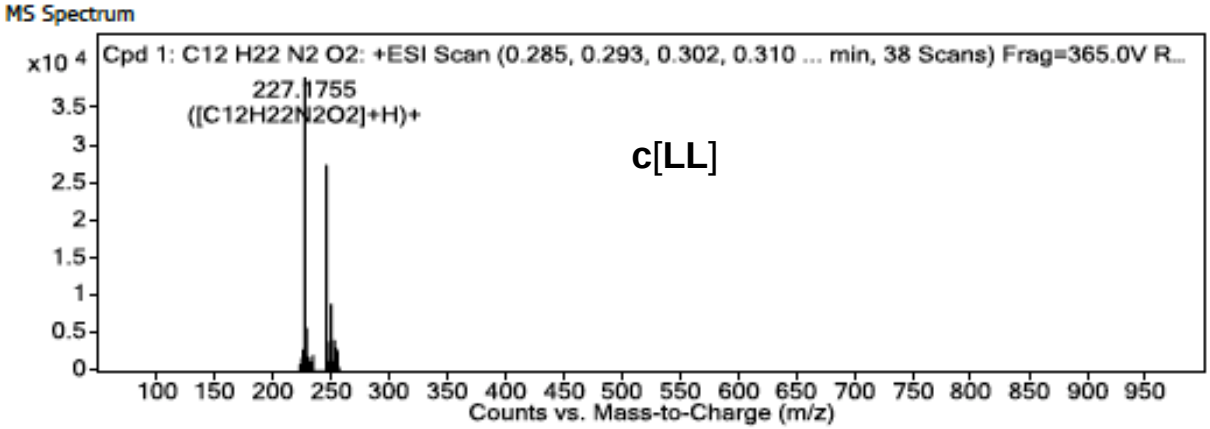
MS Spectrum
Cpd 1: C12 H22 N2 O2: +ESI Scan (0.285, 0.293, 0.302, 0.310 ... min, 38 Scans) Frag=365.0V R...
x10 4
227.1755
([C12H22N2O2]+H)+
c[LL]
Counts vs. Mass-to-Charge (m/z)

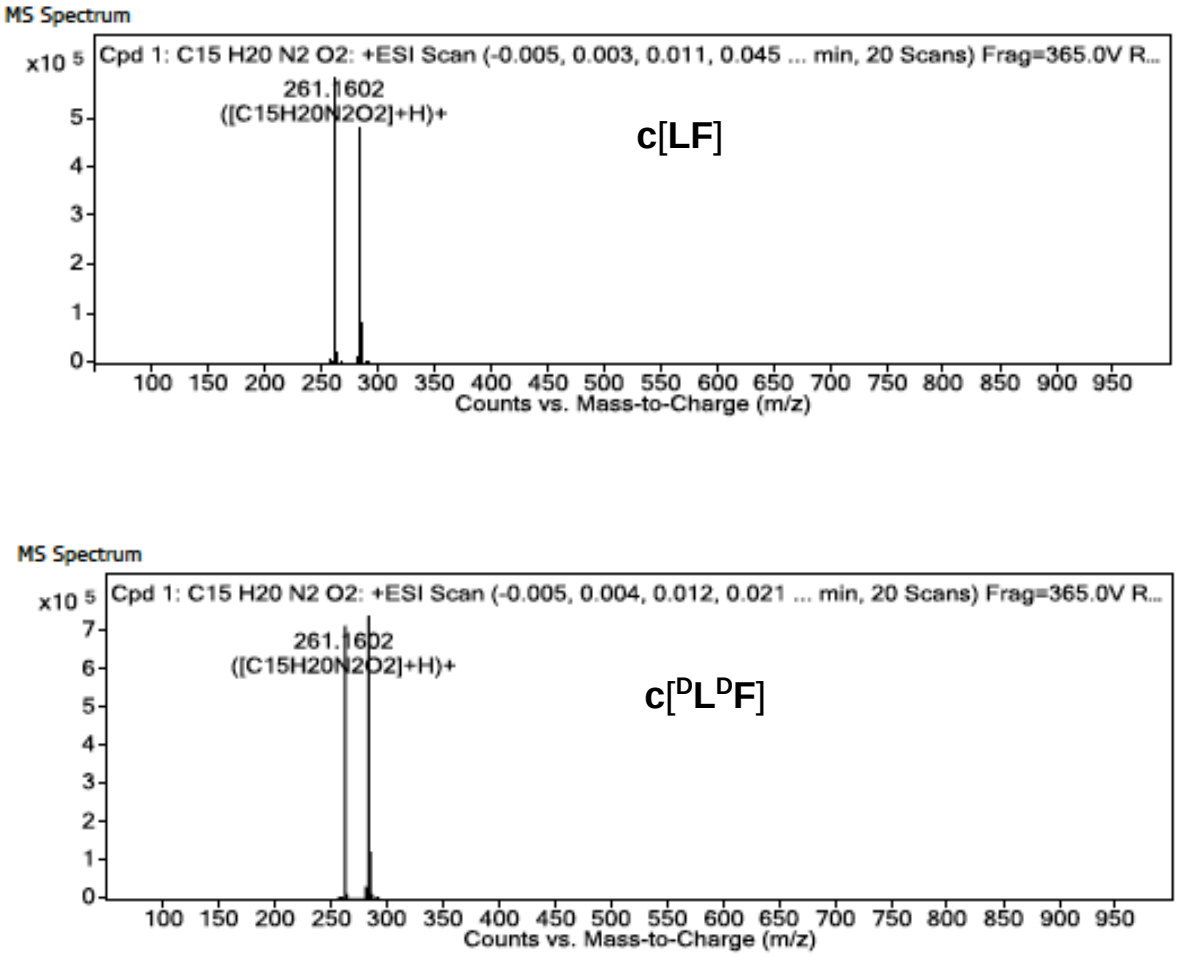

Figure S2. MS spectra of cyclic dipeptides formed after 7 days.

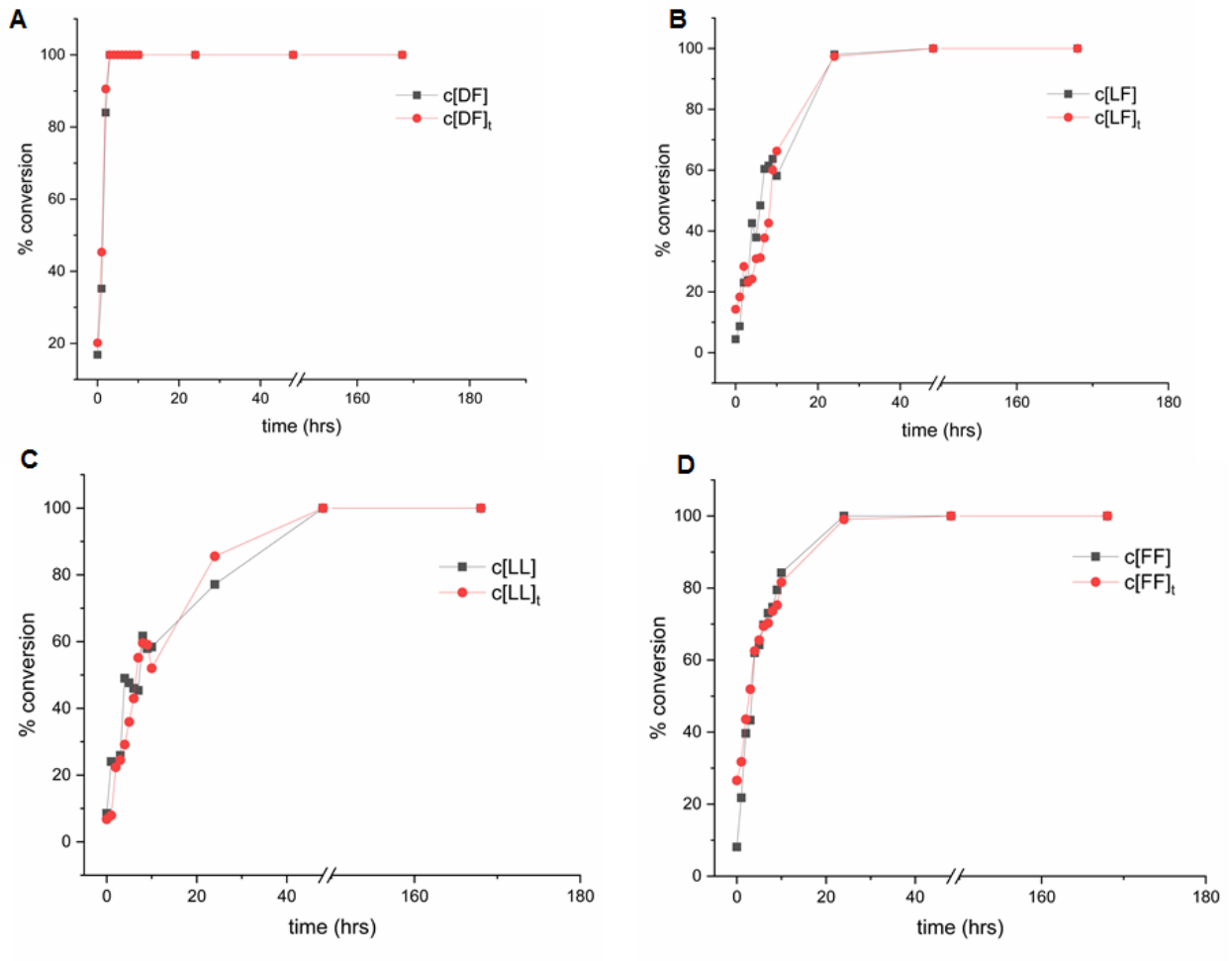

Figure S3. Kinetics of formation of the cyclic peptides made from 20 mmol kg^{-1} dipeptide esters in 100 mM phosphate buffer pH 8 in the absence (black symbols) and presence (red symbols) of 5 mol % of the corresponding preformed cyclic dipeptide. A) c[**DF**], B) c[**LF**], C) c[**LL**] and D) c[**FF**].

^{1}H NMR data

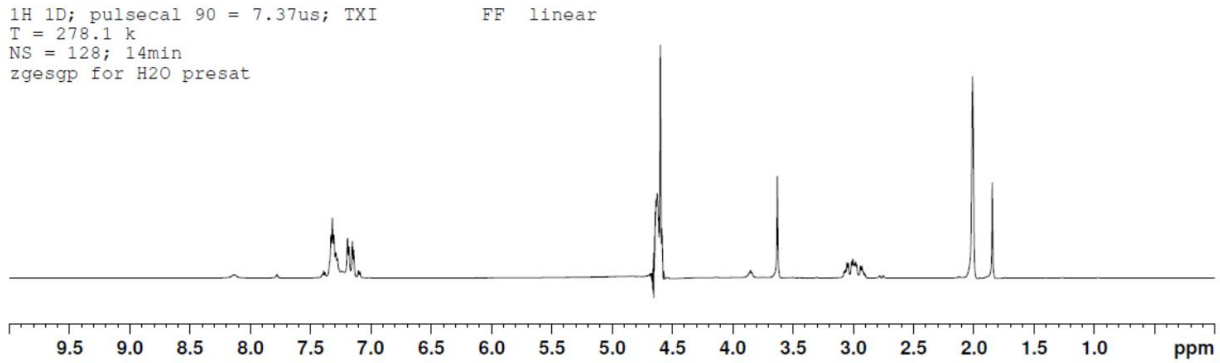

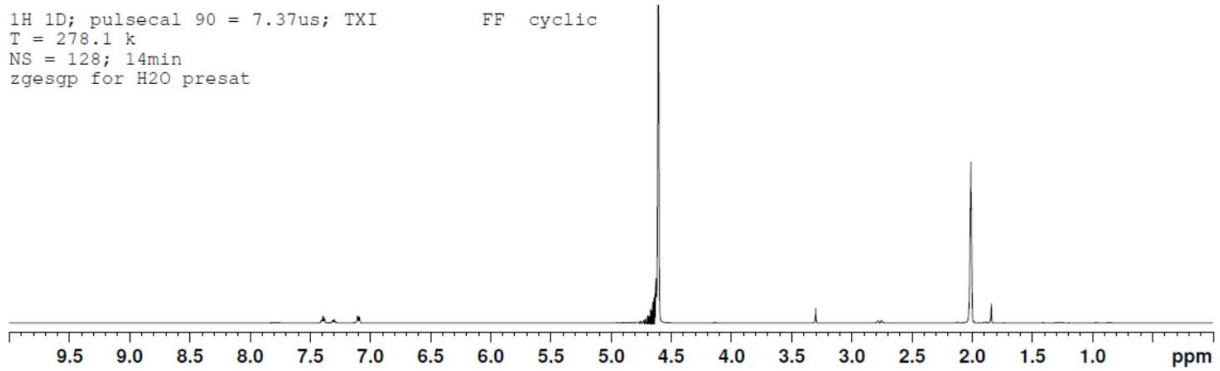

FF-OMe

^{1}H NMR (600 MHz, 50% H_2O: 50% CD_3CN): δ 7.3 (m, 5H, j=7.02), δ 7.1 (m, 5H, J=7.02), δ 3.86 (t, 1H, J=7.02), δ 3.62 (3H), δ 2.98 (m, 6H, J=7.74)

c[FF]

^{1}H NMR (600 MHz, 50% H_2O: 50% CD_3CN): δ 7.38 (t, 4H, j=7.8), δ 7.31 (t, 2H, J=7.5), δ 7.1 (d, 4H, J=8.04), δ 1.8 (d, 4H, J=3.96)

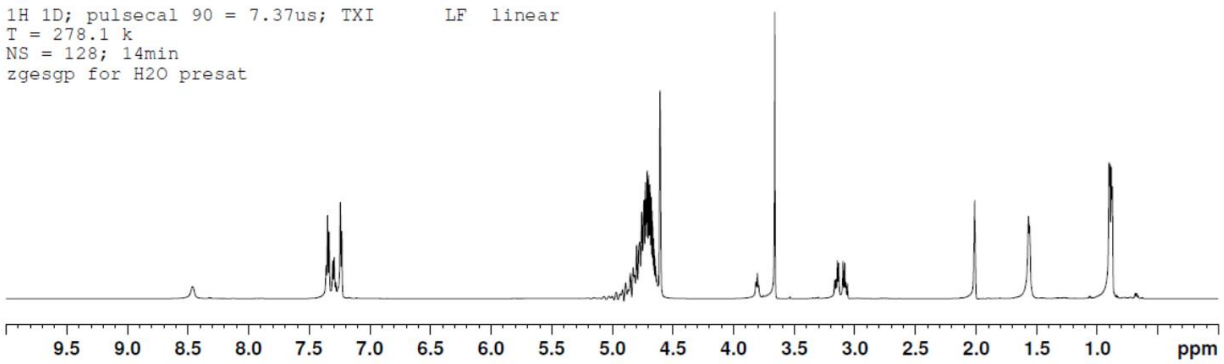

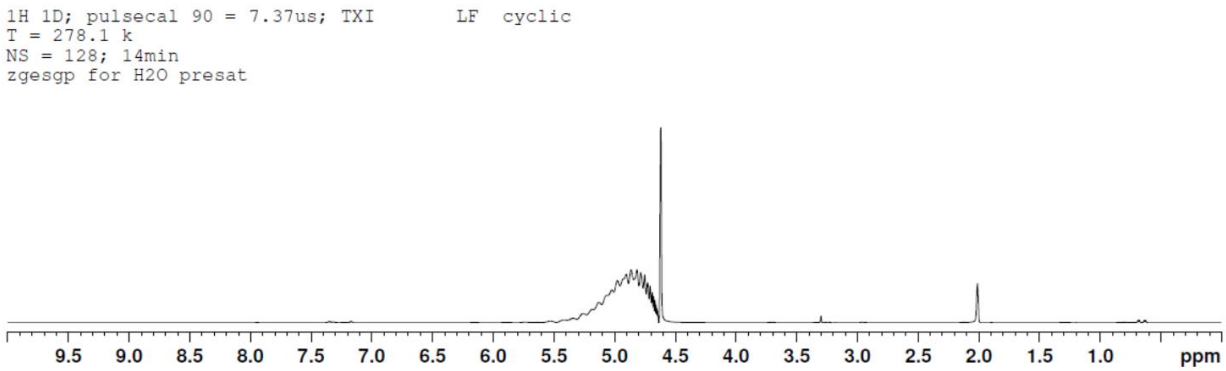

LF-OMe

^{1}H NMR (600 MHz, 50% H_2O: 50% CD_3CN): δ 7.35 (t, 2H, j=7.22), δ 7.31 (t, 1H, J=7.31), δ 7.25 (d, 2H, J=7.86), δ 3.66 (3H), δ 2.01 (m, 1H, J=2.34), δ 1.55 (d, 3H, J=5.46), δ 0.88 (dd, 6H, J=5.88)

c[LF]

^{1}H NMR (600 MHz, 50% H_2O: 50% CD_3CN): δ 7.35 (t, 2H, j=7.2), δ 7.31 (t, 1H, J=7.32), δ 7.1 (d, 2H, J=8.28), δ 3.69 (t, 1H, J=2.8), δ 3.23 (t, 1H, J=2.7), δ 1.28 (t, 1H, J=6.24), δ 0.84 (m, 1H, J=6.84), δ 0.68 (d, 3H, J=7.92), δ 0.62 (d, 3H, J=7.14)

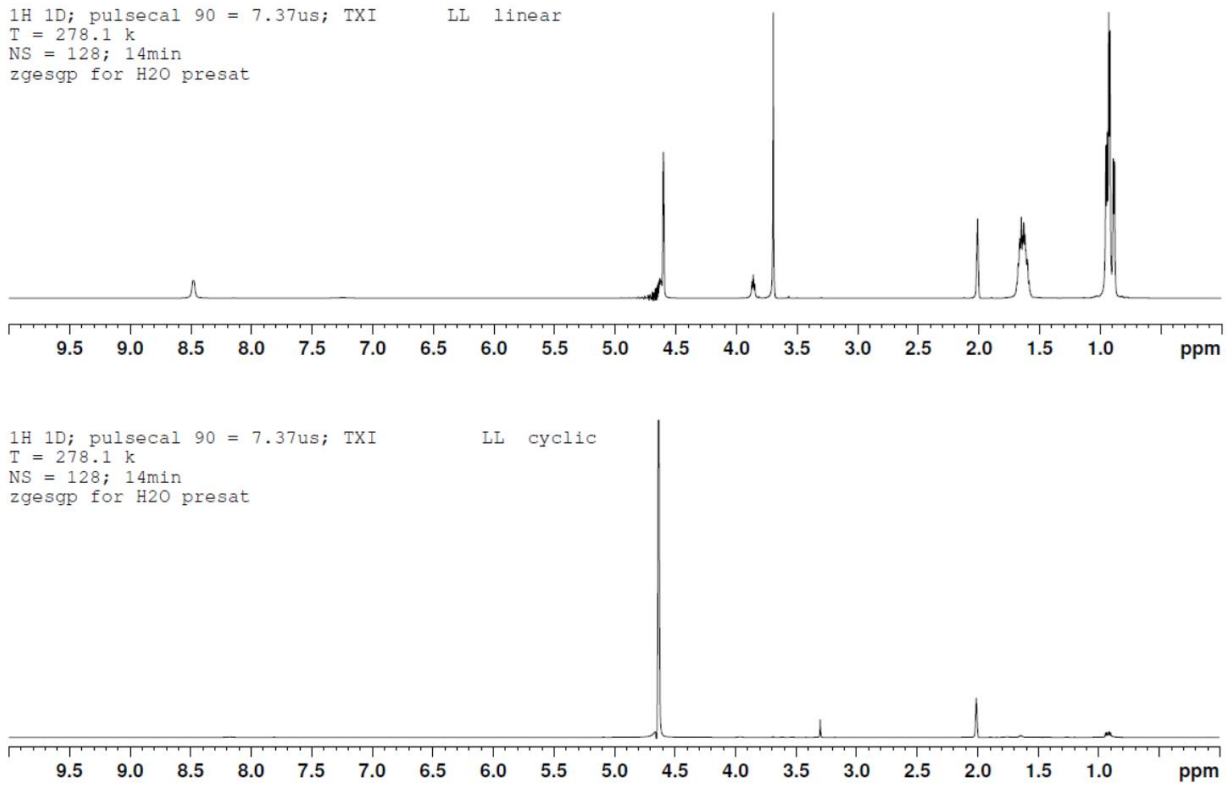

LL-OMe

^{1}H NMR (600 MHz, 50% H_2O: 50% CD_3CN): δ 3.86 (t, 1H, j=7.68), δ 3.7 (3H), δ 2.00 (t, 2H, J=2.28), δ 1.65 (m, 7H, J=6.78), δ 0.92 (m, 12H, J=6.24)

c[LL]

^{1}H NMR (600 MHz, 50% H_2O: 50% CD_3CN): δ 1.64 (t, 2H, j=5.76), δ 0.94 (d, 6H, J=6.84), δ 0.92 (d, 6H, J=6.66)

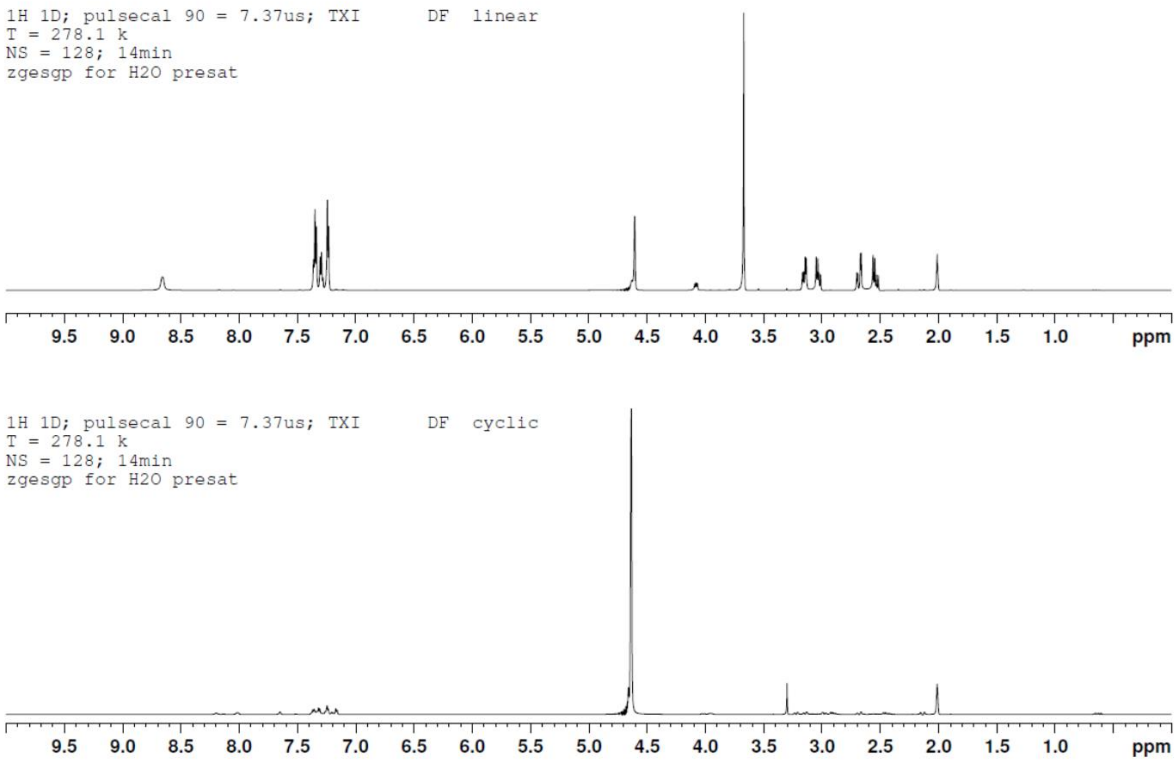

DF-OMe

^{1}H NMR (600 MHz, 50% H_2O: 50% CD_3CN): δ 7.34 (t, 2H, j=8.16), δ 7.29 (t, 1H, J=7.32), δ 7.24 (d, 2H, J=5.58), δ 3.67 (3H), δ 3.15 (dd, 1H, J=6.9), δ 3.04 (dd, 1H, J=8.34), δ 2.08 (t, 1H, J=2.76)

c[DF]

^{1}H NMR (600 MHz, 50% H_2O: 50% CD_3CN): δ 7.4-7.1 (m, 5H, j=7.44), δ 2.9 (t, 1H, J=6), δ 2.4 (t, 1H, J=6)

Figure S4. ^{1}H NMR spectra of linear methyl esters (top panel) and cyclic dipeptides (bottom panel) after 3 days of the reaction.

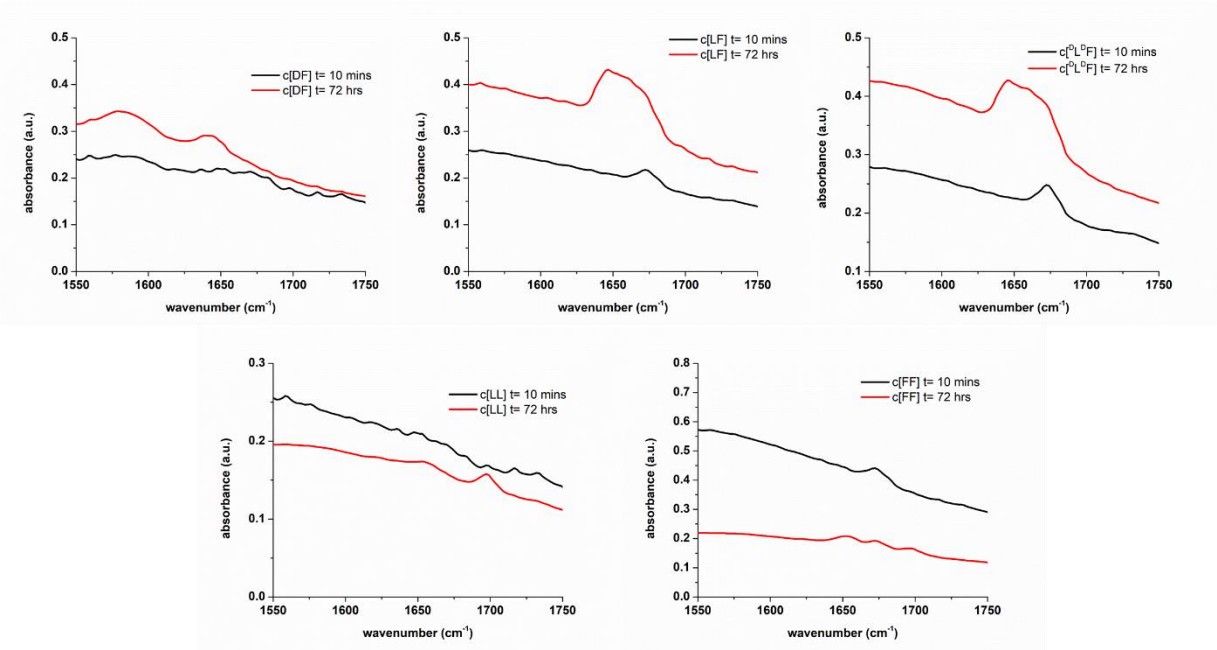

Figure S5. FT-IR spectra of the cyclic dipeptides at 10 minutes and after 72 hours of the reaction.

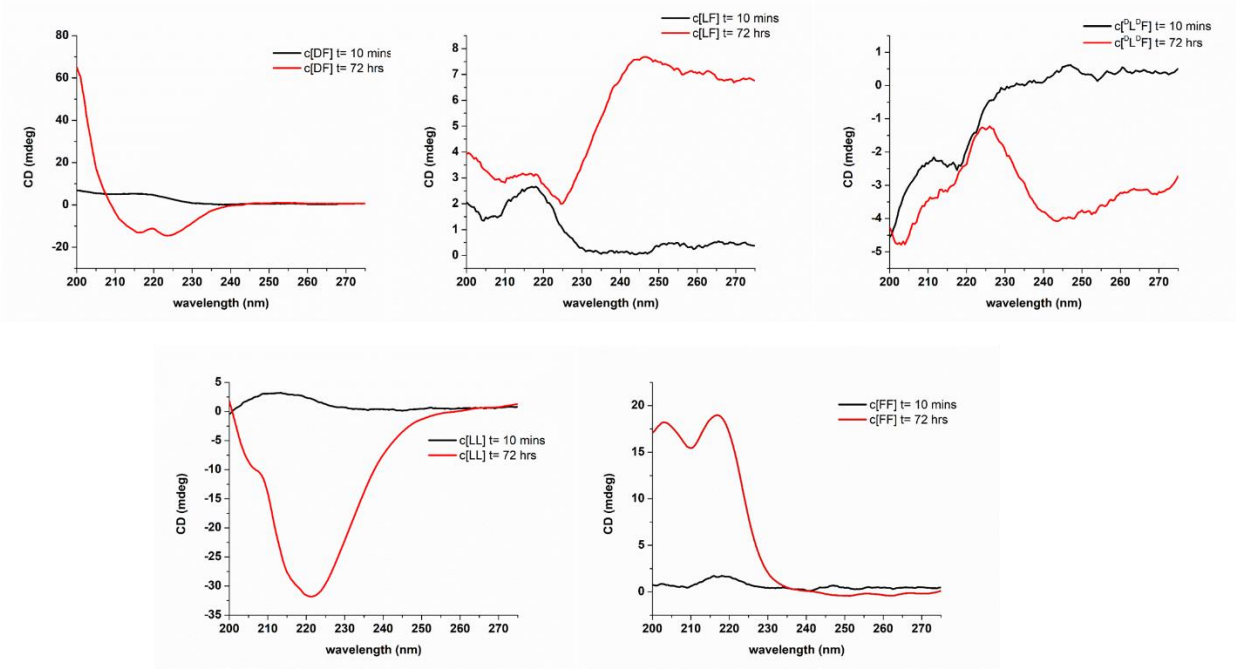

Figure S6. CD spectra of the cyclic dipeptides at 10 minutes and after 72 hours of the reaction.

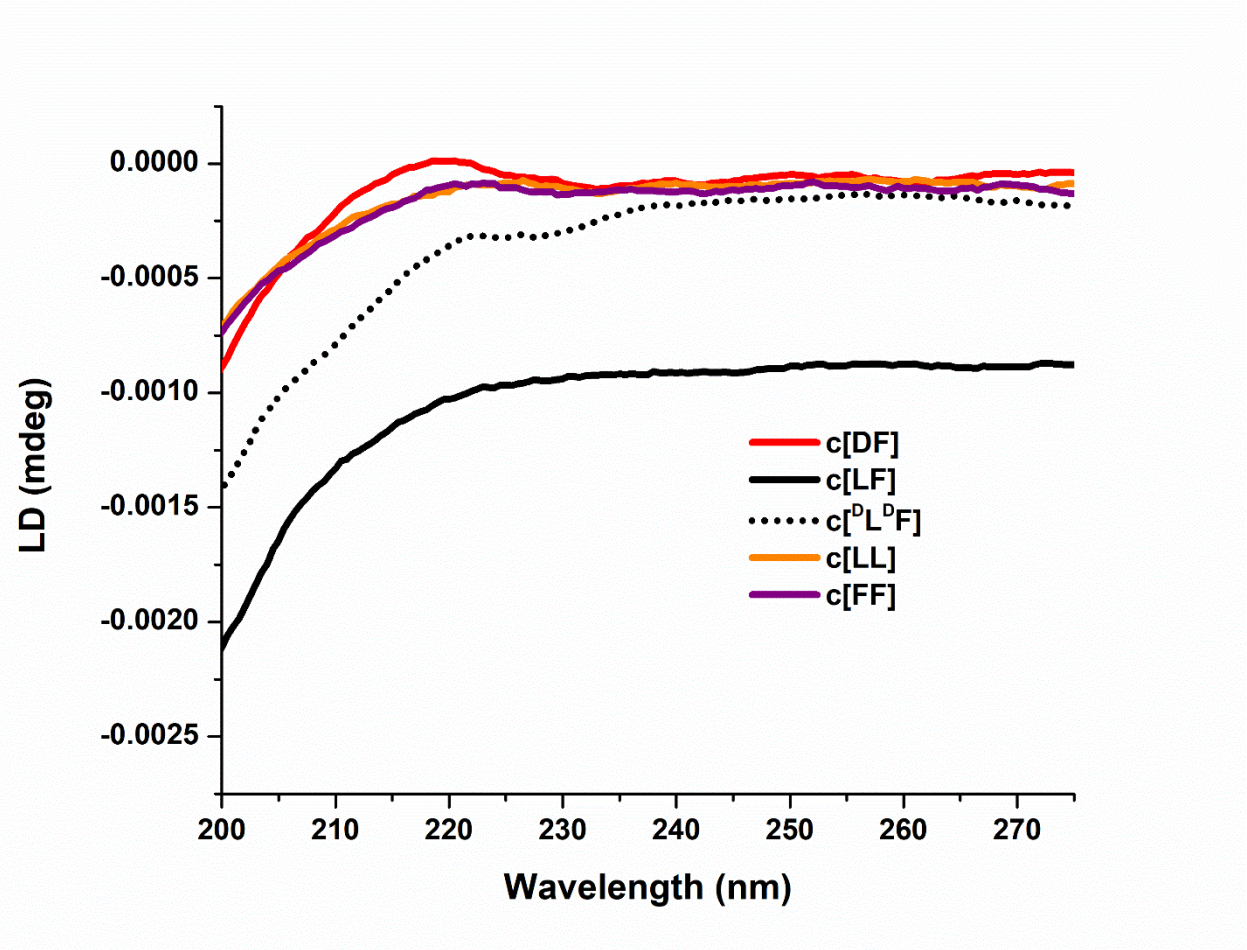

Figure S7. LD spectra of cyclic dipeptides.

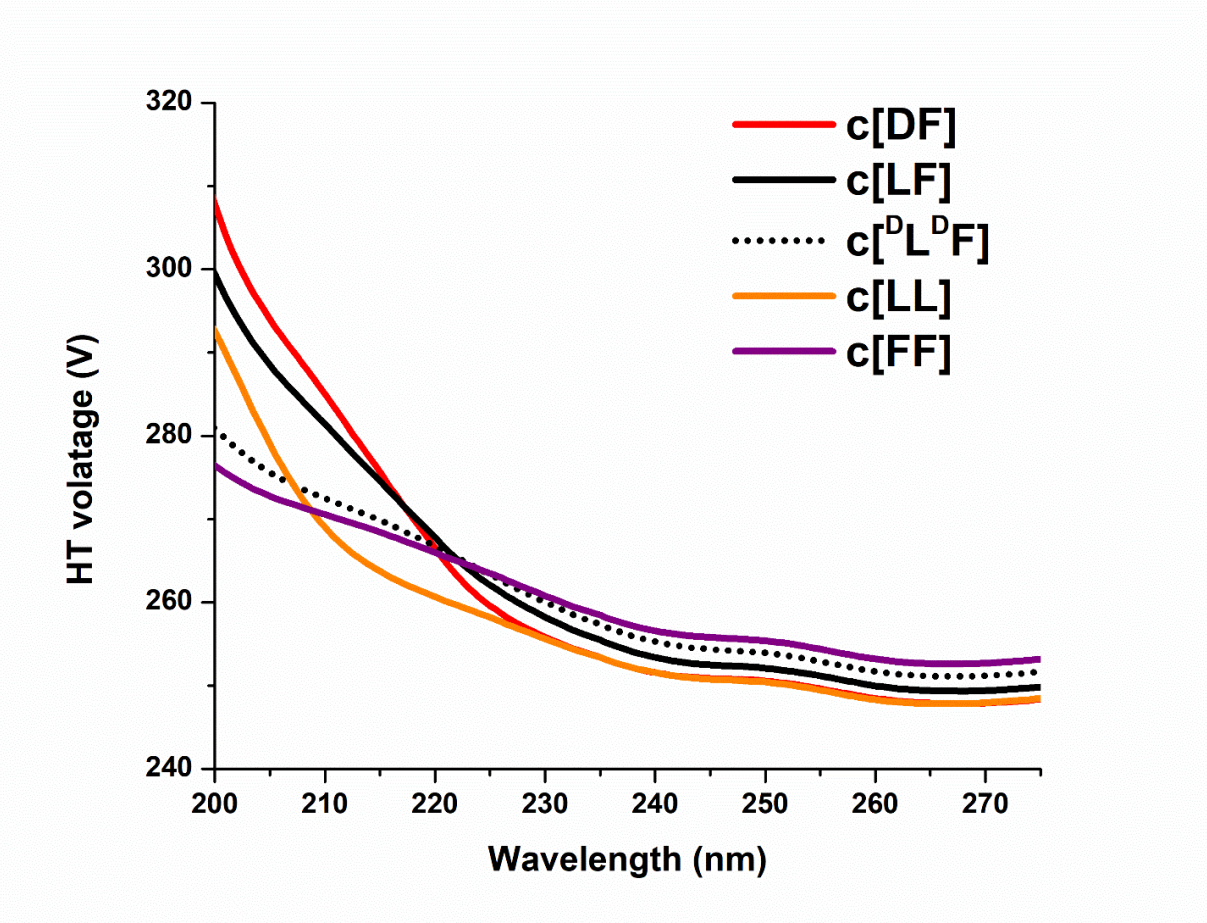

Figure S8. HT values of CD signals of the cyclic dipeptides presented in Figure 1D.

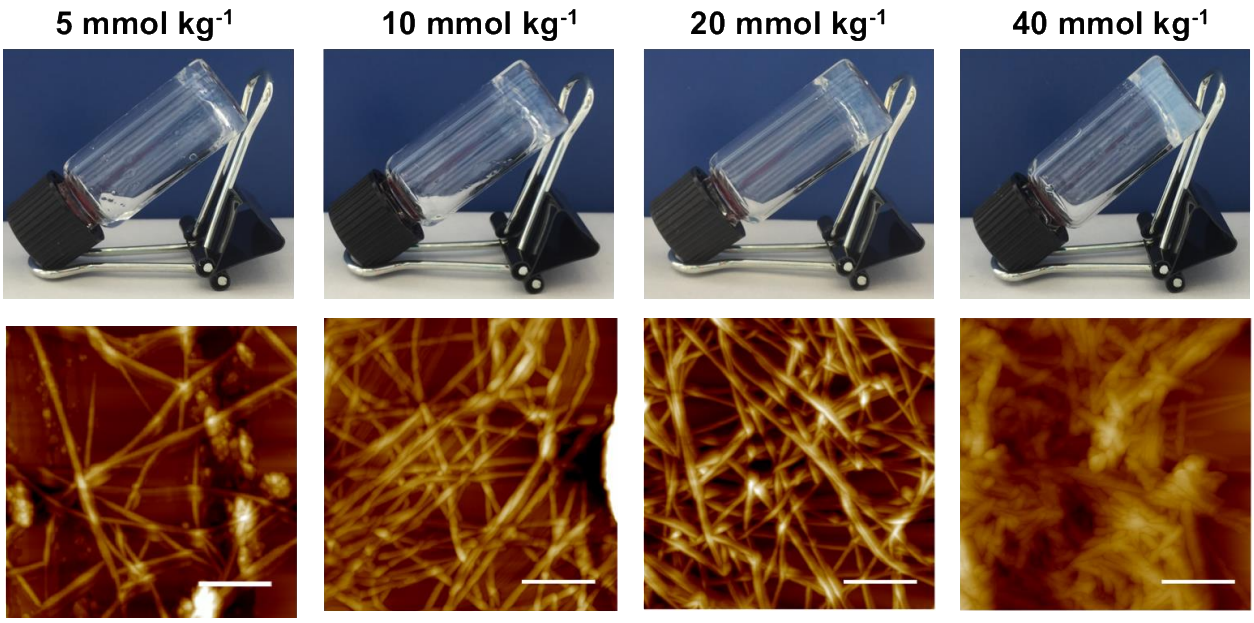

Figure S9. c[**LF**] hydrogels at different concentrations and their respective AFM images, scale bar 500 nm.

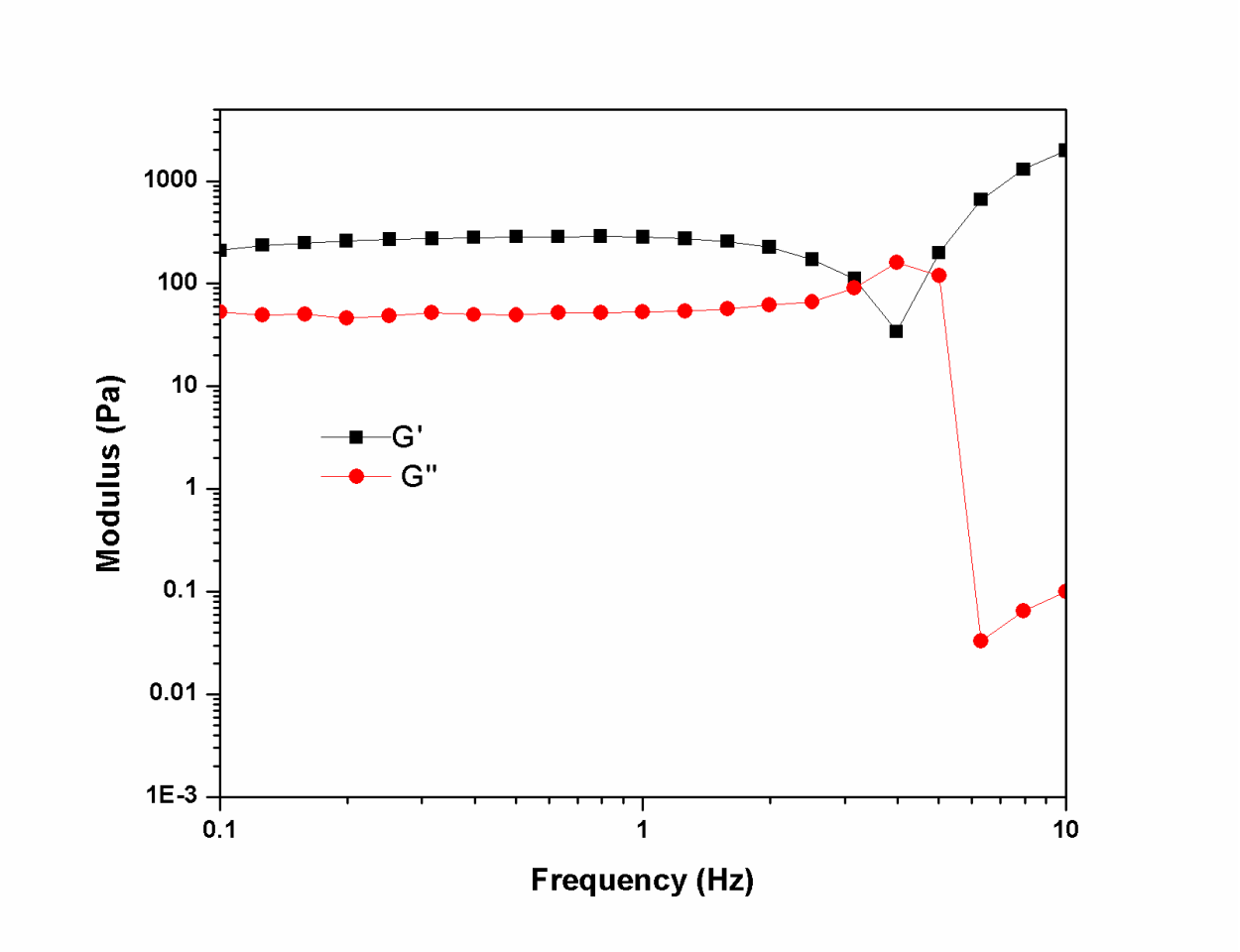

Figure S10. Rheological data of 5 mmol kg^{-1} of c[**LF**] in 100 mM sodium phosphate buffer pH 8.

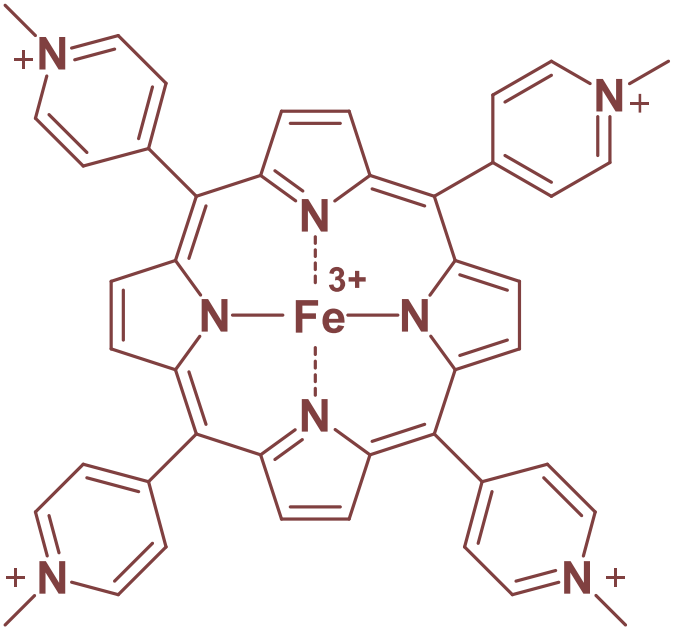

Figure S11. Chemical structure of Fe^{III}-TMPyP.

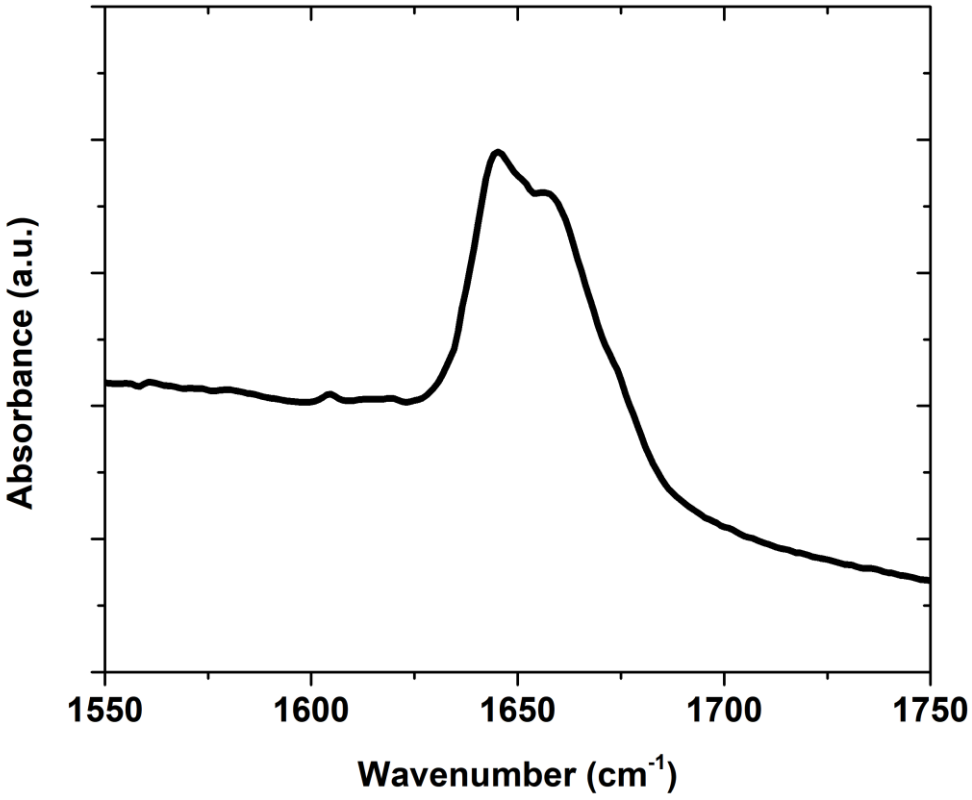

Figure S12. FT-IR spectrum of c[**LF**] after 72 hours of co-assembly with Fe^{III}-TMPyP.

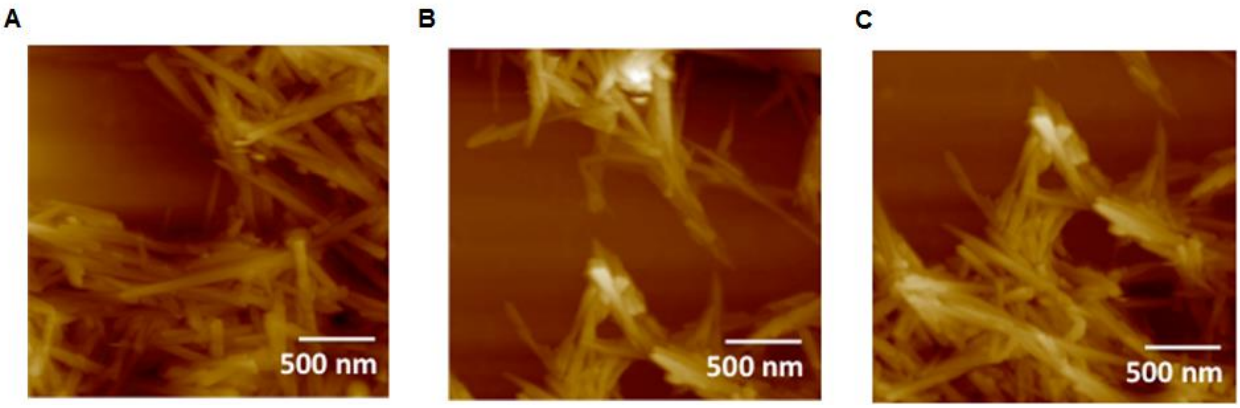

Figure S13. AFM images of A) c[**DF**]-Fe^{III}-TMPyP, B) c[**LL**]-Fe^{III}-TMPyP and C) c[**FF**]-Fe^{III}-TMPyP.

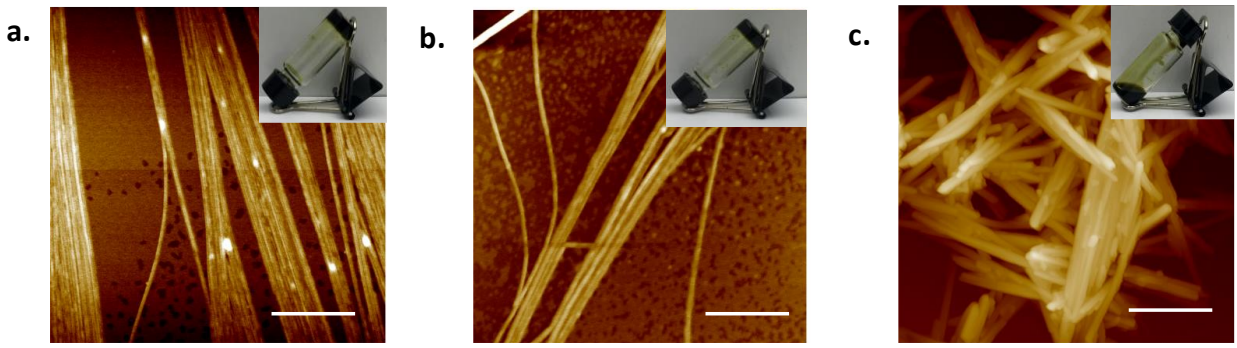

Figure S14. AFM images generated from co-assembly between Fe^{III}-TMPyP and a. c[**LF**], b. c[^{D}**L**^{D}**F**] and c. Fe^{III}-TMPyP (control). The concentration of c[**LF**] or c[^{D}**L**^{D}**F**] was 20 mmol kg^{-1}, while Fe^{III}-TMPyP was 2 mM. The digital images show the macroscopic behavior after 72 hours of reaction. Scale bar 500 nm.

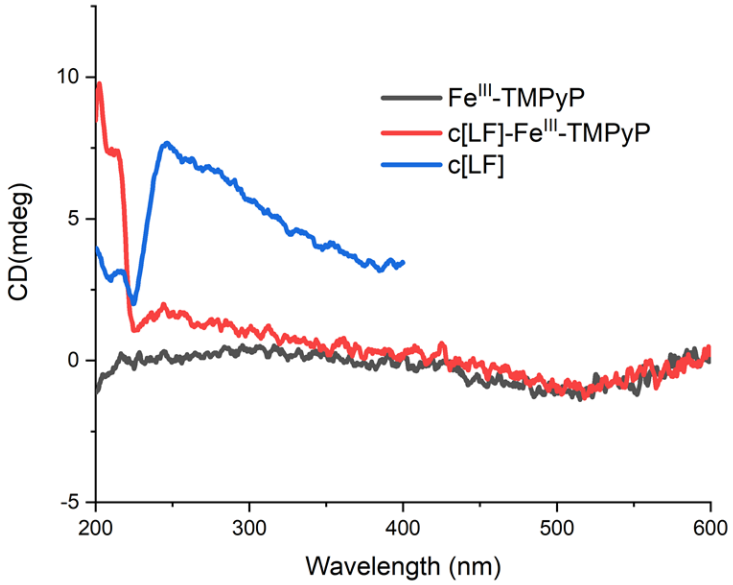

Figure S15. CD spectra of c[**LF**]-Fe^{III}-TMPyP (red line). Spectra of c[**LF**] (blue line) and Fe^{III}-TMPyP (black line) are given for comparison.

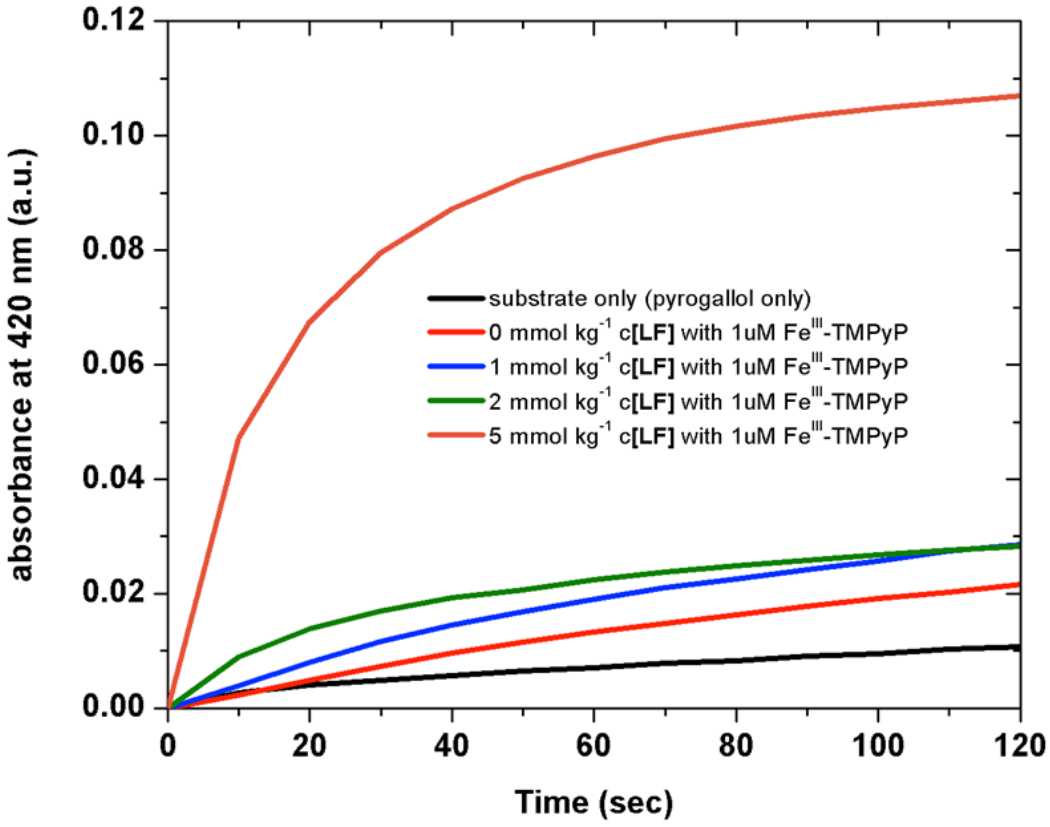

Figure S16. Time-dependent oxidation of pyrogallol (120 seconds) catalyzed by c[**LF**]-[Fe^{III}-TMPyP] nanostructures**.** A zero-minute run was done at 420 nm (before adding the H_2O_2 and pyrogallol for the catalytic reaction to initiate) to ensure that the absorbance of Fe^{III}-TMPyP does not contribute to the absorbance of product formation from oxidation of pyragallol. The initial absorbance was subtracted from each run after the oxidation was monitored.

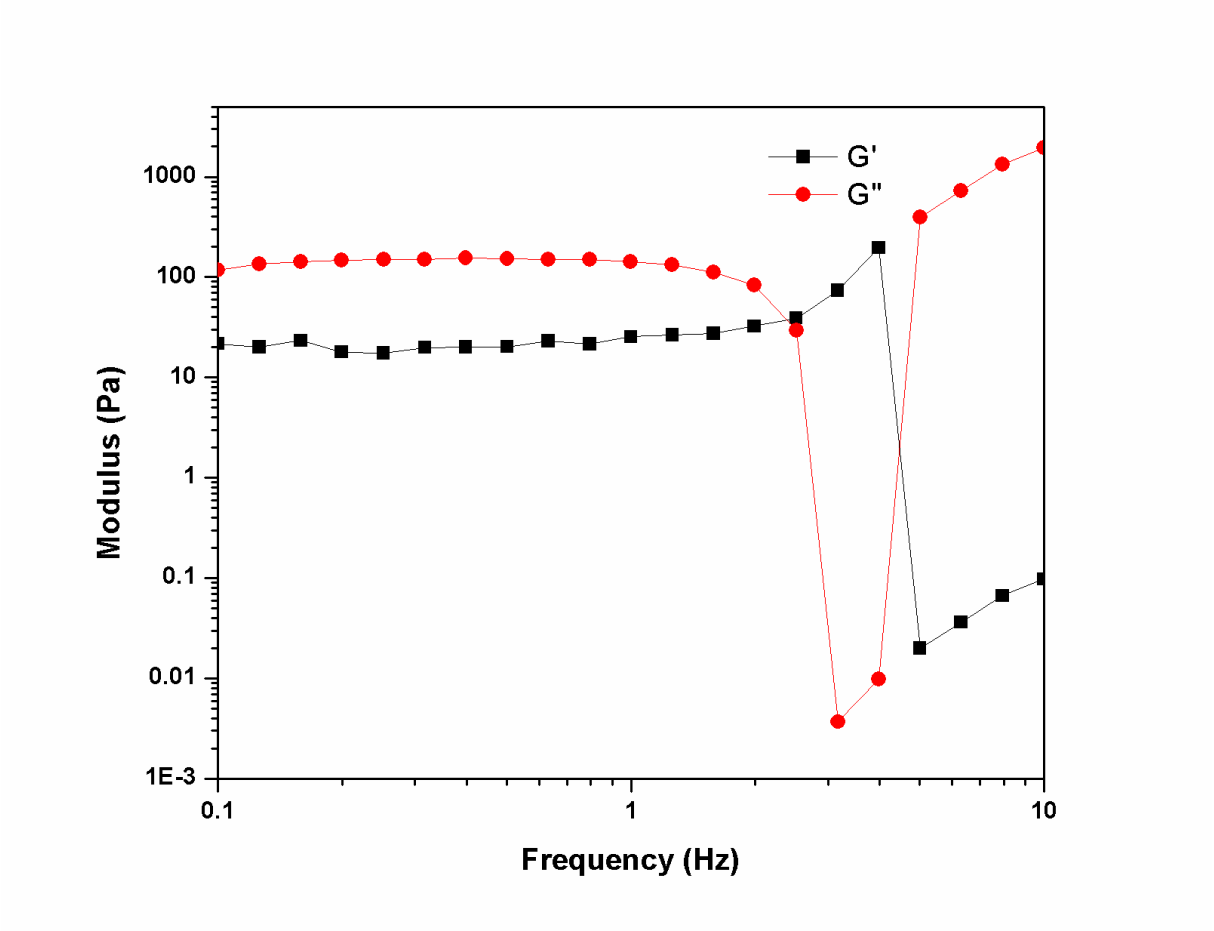

Figure S17. Rheological data of 5 mmol kg^{-1} of c[**LF**] in the presence of 1 μM Fe^{III}–TMPyP in 100 mM sodium phosphate buffer pH 8.